

REVIEWS OF TOPICAL PROBLEMS

PACS numbers: 12.38.Aw, 12.38.Ge, 25.75.Nq

Color confinement and hadron structure in lattice chromodynamics

V G Bornyakov, M I Polikarpov, T Suzuki, M N Chernodub, G Schierholz

DOI: 10.1070/PU2004v047n01ABEH001605

Contents

Abstract. Results of a recent supercomputer analysis of lattice QCD with dynamical fermions are presented. Gluon fields inside mesons and baryons with static (infinitely heavy) quarks are described. The breaking, due to the creation of a quark – antiquark pair from a vacuum, of the string that couples quarks into hadrons is discussed. The finite temperature QCD phase transition is considered. The results obtained show that the QCD vacuum behaves as a dual superconductor and that color confinement is due to the formation of a dual analog of the Abrikosov string.

V G Bornyakov Russian State Research Center "Institute of Theoretical and Experimental Physics" B. Cheremushkinskaya 25, 117259 Moscow, Russian Federation
Tel. (7-095) 129 95 73. Fax (7-095) 127 08 33
Russian State Research Center "Institute for High Energy Physics" 142284 Protvino, Moscow Region, Russian Federation
Tel. (7-0967) 713 559. Fax (7-0967) 742 874
E-mail: bornvit@sirius.ihep.su
M I Polikarpov, M N Chernodub
Russian State Research Center
"Institute of Theoretical and Experimental Physics"
B. Cheremushkinskaya 25, 117259 Moscow, Russian Federation
Tel. (7-095) 129 95 73. Fax (7-095) 127 08 33
E-mail: polykarp@heron.itep.ru
T Suzuki Institute for Theoretical Physics, Kanazawa University, Kanazawa 920-1192, Japan
Tel. (+81) 76 264 5680. Fax (+81) 76 264 5741
E-mail: suzuki@hep.s.kanazawa-u.ac.jc
G Schierholz Deutsches Elektronen-Synchrotron DESY D-22603 Hamburg, Germany, John von Neumann-Institüt für Computing NIC, Deutsches Elektronen-Synchrotron DESY, D-15738 Zeuthen, Germany
Tel. (+44) 33 762 77 238
Fax (+44) 33 762 74 413
E-mail: Gerrit.Schierholz@desy.de

Received 24 March 2003, revised 30 August 2003
Uspekhi Fizicheskikh Nauk **174** (1) 19 – 38 (2004)
Translated by G Pontecorvo; edited by A Radzig

1. Introduction

At present, analytical calculations in quantum chromodynamics (QCD) are self-consistent only in the ultraviolet region within the framework of perturbation theory, while the most interesting problems such as, say, the development of the theory of color confinement, computation of the hadron mass spectrum, and other nonperturbative problems have no analytical solutions following directly from the QCD Lagrangian. It is well known that a physical quantity M exhibiting the dimensionality of mass must depend on the bare charge g of the theory in the limit of small g as follows:

$$M \propto \exp\left(-\frac{\text{const}}{g^2}\right). \tag{1}$$

Since the dependence of M upon g is not analytical, it is impossible to apply perturbation theory for calculating quantities such as hadron masses. Only numerical computations by supercomputers permit us to obtain the dependence (1) directly from the QCD Lagrangian. In spite of known achievements in describing nonperturbative phenomena with the aid of sum rules, the instanton vacuum model, the method of field correlators, and so on, it has not been possible to obtain hadron masses in the form of dependence (1). Any such result would point to a significant development in field theory. For instance, an analytical proof of the existence of a gap in the spectrum of gluodynamics (of the nonzero mass of the lightest excitation — the glueball) is one of the 'problems of the millennium', and a prize of one million dollars is to be awarded for its resolution (for details see the Internet site http://www.claymath.org/Millennium_Prize_Problems/).

Thus, at present, a number of problems in quantum field theory can only be resolved numerically. The numerical method for investigation of lattice QCD has taken shape very well and represents a rapidly developing field of study. This approach is expected to make possible the solution to the following problems:

• to compute the hadron mass spectrum, the coupling constant α_s, and the masses of light quarks;

• to predict the low-energy behavior of various matrix elements, accounting for strong interactions;

• to predict masses of exotic states, glueballs, hybrids, etc.;

• to draw the phase diagram of quark – gluon matter in the $\mu - T$ (chemical potential – temperature) plane;

• to obtain exhaustive information on the mechanism of color confinement and (if we are lucky) to develop a theory of this phenomenon.

These problems are already being partially resolved within the framework of the lattice approach: the mass spectrum of the lightest hadrons coincides, within the errors, with the experimental values (see Section 2.2), and investigation of lattice theories in the Abelian projection has permitted us to develop a model for color confinement (see Section 3.1).

The results presented in this review have been obtained during the past two years by the collaboration DIK (DESY-ITEP-Kanazawa University) [1 – 4]. The outline of the review is as follows. The main definitions of lattice theory are presented in Section 2. Section 3 is devoted to a description of gluon fields inside a meson. The same fields are described in Section 4 in the case of finite temperatures; discussed, also, are string breaking due to the production of a quark – antiquark pair from a vacuum and the phase transition (crossover) temperature. In Section 5, a description is presented of gluon fields in baryons at zero and finite temperatures. Note that in studying gluon fields in mesons and baryons it is convenient to exclude the motion of quarks, so we consider mesons and baryons composed of infinitely heavy quarks. The main results of the papers discussed in this review are formulated in Section 6.

2. Lattice theories

2.1 Main definitions

To perform numerical QCD calculations it is necessary to pass from continuum theory in Minkowski space to lattice theory in Euclidean space. To this end, Wick rotation is performed, imaginary time is substituted for time, $t \to \mathrm{i}t$, and the generating functional $\mathcal{Z}$ of the theory (the Feynman integral) becomes similar to a statistical sum:

$$\mathcal{Z} = \int \exp\left\{\mathrm{i}S_{\mathrm{M}}[\varphi]\right\} \mathcal{D}\varphi \to \int \exp\left\{-\,S[\varphi]\right\} \mathcal{D}\varphi\,, \qquad (2)$$

where S_{M} and S are the actions in Minkowski and Euclidean spaces, respectively. The similarity to statistical physics becomes quite complete upon transition to discrete space-time. Here, finite four-dimensional Euclidean space, $0 < x, y, z, t \leqslant R$, is dealt with, and coordinates are considered to assume discrete values. Thus, one obtains a four-dimensional lattice with sites at the points $s = (x_1, x_2, x_3, x_4)$, $1 \leqslant x_k \leqslant L = R/a$, with a being the lattice spacing. The generating functional of the theory is now reduced to a finite-dimensional integral

$$\mathcal{Z} = \int \prod_s \mathrm{d}\varphi(s) \exp\left\{-\,S[\varphi]\right\}. \qquad (3)$$

Transfer from continuum integration to integration over $\varphi(s)$ makes it possible to calculate quantum averages numerically. The continuum limit corresponds to $L \to \infty$ and $a \to 0$, while in reality calculations are performed for finite L and a, and systematic errors are estimated in a standard way: by varying the number of lattice sites L^4 and the lattice spacing a.

For the QCD Lagrangian

$$\mathcal{L} = \frac{1}{2g^2}\,\mathrm{Tr}\,F_{\mu\nu}^2(x) - \sum_f \bar\psi_f(x)(D_\mu\gamma_\mu + m_f)\,\psi_f(x)\,, \qquad (4)$$

where ψ_f, $\bar\psi_f$ are the quark fields with flavor f, $F_{\mu\nu}$ is the gauge field strength tensor, D_μ is the covariant derivative, γ_μ are the Dirac matrices, and m_f is the quark mass, the definition of its lattice analogue is ambiguous. Two requirements, to be imposed on the lattice Lagrangian, are evident:

• gauge invariance;

• a correct (naive) continuum limit: the lattice Lagrangian must transform into the continuum Lagrangian (4), as $a \to 0$.

These two requirements are satisfied by an infinite number of lattice Lagrangians. The most simple and most natural form of lattice action was proposed by Wilson [5]:

$$S = S_{\mathrm{W}}^{\mathrm{G}} + S_{\mathrm{W}}^{\mathrm{F}}\,, \qquad (5)$$

where

$$\begin{aligned} S_{\mathrm{W}}^{\mathrm{F}} &= a^4 \sum_s \bar\psi(s)\,\psi(s) \\ &+ \varkappa a^3 \sum_{s,\mu} \bar\psi(s)\big[(\gamma_\mu - r)\,U_\mu(s)\,\psi(s+\hat\mu) \\ &- (\gamma_\mu + r)\;U_\mu^\dagger(s-\hat\mu)\,\psi(s-\hat\mu)\big] \end{aligned} \qquad (6)$$

is the fermion part of the action for a single flavor, while

$$S_{\mathrm{W}}^{\mathrm{G}} = \beta \sum_P \left(1 - \frac{1}{3}\,\mathrm{Re}\,\mathrm{Tr}\,U_P\right) \qquad (7)$$

represents the action of the gauge fields, $\varkappa$ is a parameter determining the quark mass, and $\beta = 6/g^2$ is the lattice coupling constant. The 'plaquette' matrix U_P is constructed in a standard way from link variables $U_\mu(s) = \exp\left[\mathrm{i}a\hat A_\mu(s)\right]$, where $\hat A_\mu(s)$ is the SU(3) gauge field. The Wilson fermion action tends toward a continuum limit more slowly than the action of gauge fields:

$$\begin{aligned} S_{\mathrm{W}}^{\mathrm{G}} &\xrightarrow{a\to 0} \frac{1}{2\,g^2}\int \mathrm{Tr}\,F_{\mu\nu}^2\,\mathrm{d}^4x + O(a^2)\,, \\ S_{\mathrm{W}}^{\mathrm{F}} &\xrightarrow{a\to 0} \int \bar\psi(D_\mu\gamma_\mu + m)\,\psi\,\mathrm{d}^4x + O(a)\,. \end{aligned} \qquad (8)$$

This disadvantage is removed in the 'improved' action for fermion fields, viz.

$$S^{\mathrm{F}} = S_{\mathrm{W}}^{\mathrm{F}} - \frac{\mathrm{i}}{2}\,\varkappa g\,a^5 c_{\mathrm{SW}} \sum_s \bar\psi(s)\,\sigma_{\mu\nu}F_{\mu\nu}(s)\,\psi(s) \equiv \bar\psi\hat M\psi\,, \qquad (9)$$

where $\sigma_{\mu\nu} = [\gamma_\mu, \gamma_\nu]/(2i)$, and the parameter $c_{\rm SW}$ is determined in a nonperturbative manner [6]. The action $S^{\rm F}$ tends to a continuum limit with an accuracy $O(a^2)$, and precisely this action was applied in the calculations presented in this review.

Numerical integration can only be performed over gauge fields. Integration over fermions is performed analytically resulting in

$$\int \mathcal{D}\psi\, \mathcal{D}\bar{\psi}\, \exp\left[\bar{\psi}\hat{M}\psi\right] = \det \hat{M}\,, \tag{10}$$

and computer calculations must be carried out on an integral of the form

$$\mathcal{Z} = \int \mathcal{D}U_\mu(s) \exp\left\{-S[U_\mu(s)]\right\}, \tag{11}$$

where $S\left[U_\mu(s)\right] = S_{\rm W}^{\rm G}[U_\mu(s)] - \ln\det \hat{M}\left[U_\mu(s)\right]$, $\mathcal{D}U_\mu(s) = \prod_{s,\mu} {\rm d}U_\mu(s)$, and ${\rm d}U_\mu(s)$ is an integral over the Haar measure of the SU(3) gauge group.

Below, we only consider lattice QCD with u- and d-quarks and their masses are assumed to be equal. Thus, lattice QCD is characterized by parameters β and $\varkappa$, which determine the lattice spacing and quark mass. Actually, calculations are performed on lattices with a finite number V of sites; in the case of a symmetric lattice $V = L^4$, where L is the number of sites along one direction.

2.2 Lattice sizes and cost of simulations

The computation of integrals such as given by formula (11) in the case of real QCD is quite a difficult task. Supercomputers are utilized, and there exists a large community of physicists who invent diverse algorithms, based on the Monte Carlo method, for calculating integrals (11) as fast as possible. The discussion of these algorithms (their description is given in review [7]) goes beyond the scope of the present review. We shall only note that for numerical calculations the integral in formula (11) is replaced by a sum over configurations of the gluon field, which are generated with the weight $\exp(-S_{\rm eff})$. Now, why are supercomputers, even up to the fastest ones, needed for lattice simulations? The following simple arguments provide an answer. Let us estimate the lattice size required for performing the real QCD calculations. If we wish to describe the structure of a baryon with an accuracy of 10%, then the linear dimension of the baryon must be on the order of ten lattice spacings. But in QCD there exist π-mesons that are approximately 10 times lighter than baryons, and about 100 lattice spacings will correspond to them. Therefore, the minimum number of sites $V = L^4 \approx 100^4$. In the case of QCD calculations on a lattice of volume L^4, integrals of multiplicity $32L^4$ over gauge fields have to be computed, while the fermion determinant being calculated is of a matrix of dimension $12L^4 \times 12L^4$. Moreover, the cost of simulations required increases more rapidly than the number of degrees of freedom, so the semiphenomenological expression for QCD calculations with two light quarks has the following form [8]:

$$\text{volume of calculations} \approx 2.8 \left(\frac{N_{\rm conf}}{1000}\right)\left(\frac{m_\pi/m_\rho}{0.6}\right)^{-6} \times \left(\frac{R}{3\ \text{fm}}\right)^5 \left(\frac{1/a}{2\ \text{GeV}}\right)^7 \text{teraflop year}\,, \tag{12}$$

where $N_{\rm conf}$ is the number of gluon field configurations, and m_π and m_ρ are the π-meson and ρ-meson masses, respectively (the ratio m_π/m_ρ determines the quark mass). For example, to generate 100 configurations with parameters $m_\pi/m_\rho = 0.6$ (i.e., with a quark mass ~ 50 MeV), $R = 3$ fm, and $1/a = 2$ GeV, 100 days of operation are required for the computer with a performance 1 teraflop. Note the large exponents in expression (12), thus indicating the rapid increase of the cost of simulations occurring as the continuum or chiral limit is approached.

From relation (12) it follows that computer calculations in lattice QCD with realistic parameters cannot be performed, yet. Calculations are performed for large values of quark masses ($\sim 50-100$ MeV), when the π-meson is not light. The obtained values of physical quantities are extrapolated with the aid of chiral perturbation theory to realistic values of the light quark mass (~ 3 MeV). An example of such an extrapolation is illustrated in Fig. 1a, from which it can be seen that the relation $m_\pi^2 \propto m_{\rm q}$ holds true within quite a broad interval of quark mass variations. The hadron mass spectrum in lattice QCD, obtained with the aid of a similar extrapolation without invoking the dynamical quarks, is presented in Fig. 1b. The real mass spectrum can be seen to be described quite well, and it is to be noted that only information on the QCD Lagrangian was actually input into the supercomputer.

Now a few words about the supercomputers used in lattice calculations. The performance of the best supercomputers increases exponentially with the year of production, as one can see from Fig. 1c. All dedicated computers listed in this figure, with the exception of the 'Earth Simulator', are intended for QCD lattice calculations. At present, the 'Earth Simulator' of the NEC company is the fastest computer, its speed amounting to about 40 teraflops. Although this supercomputer is presently used in studies of global natural phenomena, according to plans, lattice QCD calculations are also to be performed in 2004. The results presented in this review have been obtained with the serial supercomputers ES40 (HP) of Humboldt University (Germany), SR-8000 (Hitachi) of the University of Münich (Germany), SX5 (NEC) of the University of Osaka (Japan), SR-8000 of the research center KEK (Japan), as well as the first (and hitherto sole) Russian supercomputer MVS 1000M. The last machine was assembled in the year 2000 at the Joint Supercomputer Center (Moscow) and comprises 768 Alpha21264A processors combined by the high-speed network Myrinet. Detailed information on the MVS 1000M can be found on the Internet (http://www.jscc.ru). At present (February 2003), this machine occupies 74th place in the list of the fastest computers in the world (http://www.top500.org/list/).

3. Gluon fields in a meson

In this section, the results are presented concerning studies of fields inside a meson consisting of an infinitely heavy quark–antiquark pair. Thus, the quark and antiquark are considered static, which allows us to investigate the string that causes color confinement. For estimation of the influence of dynamical (virtual) quarks, strings are considered both within the full QCD[1] and within the SU(3) gluodynamics. The bare charge of the latter is chosen so as to provide for the lattice spacings in both theories to be approximately equal to each other. This permits us to consider the difference in the results to be totally due to effects originating from the

[1] For the sake of brevity, we call the Yang–Mills SU(3) theory involving quarks of two flavors with mass on the order of 100 MeV the 'full' QCD.

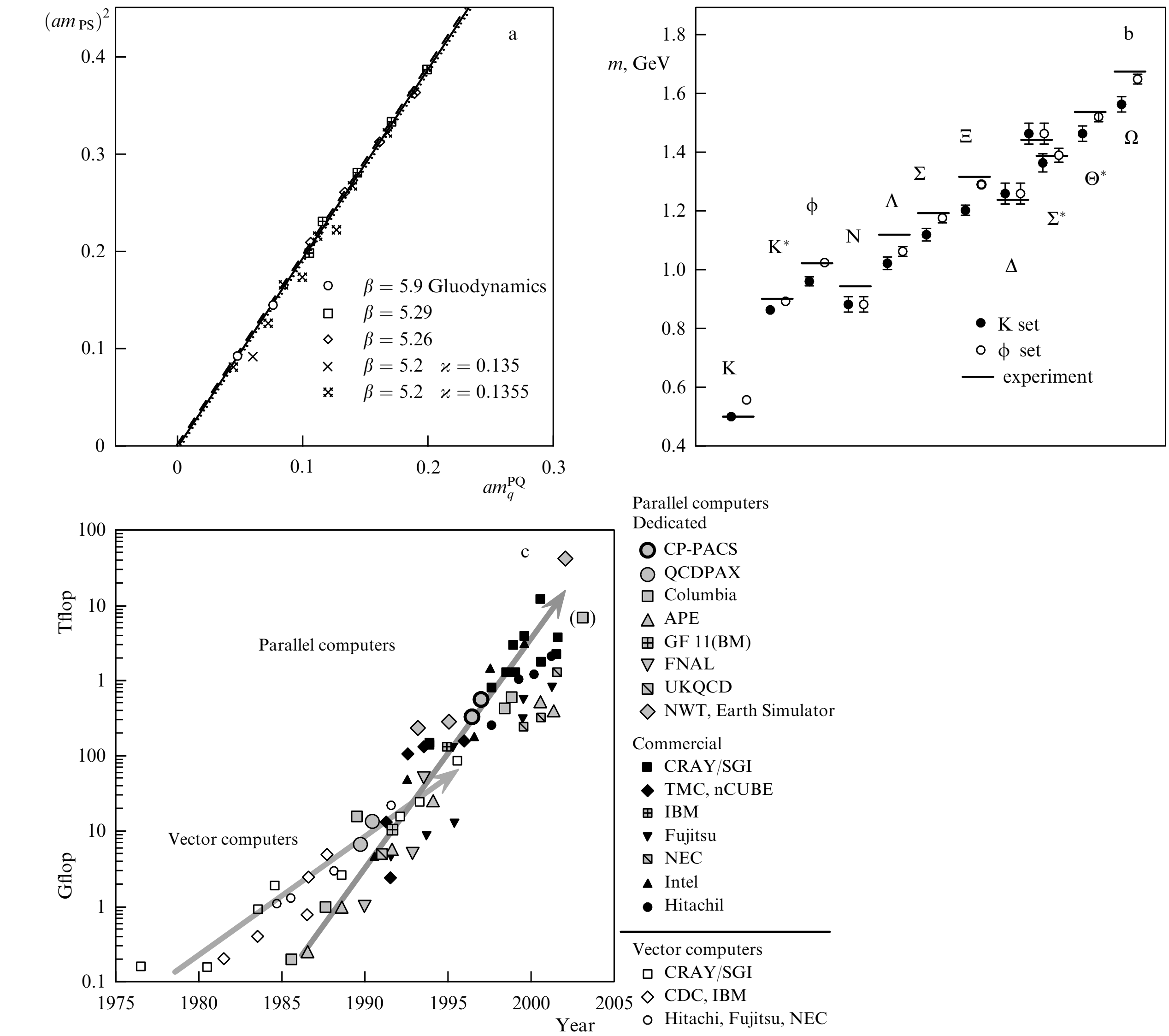

Figure 1. (a) Dependence of the square of π-meson mass, m_{π}^2, upon the quark mass m_q (the data are presented in lattice units), obtained by the UKQCD collaboration [9]. (b) Hadron mass spectrum obtained by the CP-PACS collaboration [10] within QCD without invoking the dynamical quarks. The mass of s-quarks was set equal to the experimental value of the K-meson mass or to the mass of the ϕ-meson. (c) Performance of the best supercomputers; the figure is taken from Ref. [11].

dynamical quarks. An introduction to the main definitions is followed by a brief description of the structure of vacuum fields and of the properties of the string that causes color confinement.

3.1 Simulation parameters and the maximal Abelian gauge

Calculations were performed for field configurations obtained by the QCDSF and UKQCD collaborations [12]. A total of 5 different sets of parameters were used for the full QCD, and 4 sets for QCD without virtual quarks (for gluodynamics). The characteristics of the configurations are presented in Table 1. The calculated results are conventionally expressed in terms of a 'force parameter' r_0 equal to 0.50(7) fm [13]. The continuum limit in the theory without quarks is known to be established for those values of the bare constant g, at which quantities exhibiting the dimensionality of mass depend upon g as in formula (1). In the theory with fermions, dealt with in this review, there are two parameters — the bare charge g and the bare fermion mass m, and the continuum limit is established at those values of g and m, for which 'lines of constant physics' are established in the $g-m$ plane. In this case, all the dimensional quantities can be expressed via the 'force parameter' r_0. The lines of constant physics are established with good accuracy [12] for the action with the parameters given in Table 1.

The present review deals, as a rule, with gauge fields in the Abelian projection [14], i.e., data are given only for the Abelian part of gluon fields. This procedure allows us to reduce the statistical noise by several times, and it is precisely for this reason that we have been able to investigate the structure of mesons and baryons in detail. First, the gluon fields are generated by the Monte Carlo method in accordance with expression (11), then the maximum Abelian (MA) gauge is fixed. This gauge was proposed in Ref. [15] for checking the 't Hooft – Mandelstam model of confinement [16]. In this model, monopoles condense in a vacuum, which results in squeezing of the electric fields of quarks into a tube,

Table 1. Configuration parameters.

β	$\varkappa$	m_π/m_ρ	r_0/a	a, fm	Lattice	Number of configurations
			Full QCD			
5.20	0.1355	0.6014 (96)	5.041 (40)	0.097 (1)	$16^3\times 32$	400
5.25	0.13575	0.595 (10)	5.500 (60)	0.089 (1)	$24^3\times 48$	44
5.29	0.1355	0.7095 (70)	5.595 (83)	0.088 (2)	$24^3\times 48$	52
5.29	0.135	0.7565 (44)	5.26 (7)	0.093 (2)	$16^3\times 32$	400
5.29	0.134	0.8306 (26)	4.813 (45)	0.102 (2)	$16^3\times 32$	100
			SU(3) gluodynamics			
5.8			3.665	0.137 (2)	$24^3\times 48$	30
6.0			5.368	0.091 (1)	$16^3\times 32$	175
6.0			5.368	0.091 (1)	$24^3\times 48$	30
6.2			7.383	0.068 (2)	$24^3\times 48$	30

similar to the dual Abrikosov string. The presence of the string, in turn, results in a linear potential at large distances, which provides for confinement. The 't Hooft–Mandelstam model of confinement was previously checked in SU(2) gluodynamics [17]. In the present review, results are given that confirm this model for lattice QCD.

Thus, we apply the MA gauge for calculating average values in the Abelian projection. Fixing this gauge reduces to maximization of the functional [15]

$$F[U]=\frac{1}{12V}\sum_{s,\mu}\left(\left|U_\mu^{11}(s)\right|^2+\left|U_\mu^{22}(s)\right|^2+\left|U_\mu^{33}(s)\right|^2\right), \quad (13)$$

where U_μ^{ii} are the diagonal elements of the matrix U_μ, with respect to local gauge transformations of $g(s)$: $U_\mu(s)\to U_\mu^g(s)=g(s)^\dagger U_\mu(s)\,g(s+\hat\mu)$. We have made use of the algorithm of 'Simulated Annealing' [18] for fixing the gauge. This method reduces to thermalization of the configurations $\{g(s)\}$ in accordance with the distribution

$$p(g;U)=\exp\left\{\frac{F[U^g]}{T_{\rm ext}}\right\}. \quad (14)$$

The external 'temperature' $T_{\rm ext}$ decreases from a certain initial value down to zero (in practice, down to the lowest possible value). The algorithm applied is significantly more efficient than the ordinary maximization by iterations. Nevertheless, the problem of Gribov copies, which is present in the gauge considered [19], is not fully resolved. However, the systematic error that arises owing to this problem is not large ($\approx 3\%$) [1].

3.2 Abelian variables and monopole currents

After the MA gauge is fixed, the Abelian fields are extracted from the lattice link variables $U_\mu(s)\in \mathrm{SU}(3)$ [15, 20]:

$$u_\mu(s)=\mathrm{diag}\big(u_\mu^{(1)}(s),u_\mu^{(2)}(s),u_\mu^{(3)}(s)\big)\,, \quad (15)$$

where

$$u_\mu^{(l)}(s)=\exp\left[\mathrm{i}\theta_\mu^{(l)}(s)\right],\quad \theta_\mu^{(l)}(s)\in\left[-\frac{4}{3}\,\pi,\ \frac{4}{3}\pi\right]. \quad (16)$$

The variable $u_\mu(s)$ is determined from the condition that $\left|\mathrm{Tr}\,[U_\mu^\dagger(s)\,u_\mu(s)]\right|^2$ is maximized. The functional (13) is invariant with respect to the gauge transformations $g(s)\in \mathrm{U}(1)\times\mathrm{U}(1)$, i.e., gauge freedom is not fully fixed. The Abelian variables $u_\mu(s)$ play the part of gauge fields and are transformed by the gauge transformations $\mathrm{U}(1)\times\mathrm{U}(1)$:

$$u_\mu(s)\to g(s)\,u_\mu(s)\,g^\dagger(s+\hat\mu)\,. \quad (17)$$

The theory obtained upon fixing the gauge also exhibits Weyl symmetry.

Monopole currents are determined in a standard way via the plaquette angles $\theta_P^{(l)}$ [21]:

$$k^{(l)}({}^*s,\mu)=\frac{1}{2\pi}\sum_{P\in C}\theta_P^{(l)}=\{0,\pm1,\pm2\}\,; \quad (18)$$

here, summation is performed over the oriented facets P of the cube C, which is orthogonal to the direction μ, while the site ${}^*s$ is dual to the cube C. The plaquette angles $\theta_P^{(l)}$ are calculated in the conventional manner from the link variables $\theta_\mu^{(l)}$ and then subjected to a shift so as to satisfy the condition [20]

$$\sum_{l=1}^{3}\theta_P^{(l)}=0\,. \quad (19)$$

From condition (19) follows the relation

$$\sum_{l=1}^{3}k^{(l)}({}^*s,\mu)=0\,; \quad (20)$$

therefore, only two monopole currents are independent. It should be emphasized that condition (19) does not violate the Weyl symmetry. Law of conservation of monopole currents holds valid for each color separately:

$$\sum_\mu \nabla_\mu^- k^{(l)}({}^*s,\mu)=0\,,\quad l=1,2,3\,, \quad (21)$$

where ∇_μ^- is the lattice derivative.

3.3 Monopoles in the vacuum of quantum chromodynamics

The monopole currents $k^{(l)}({}^*s,\mu)$ being conserved form clusters [22] on the dual lattice. In Refs [22, 23], these clusters were found to be divided into two classes in SU(2) gluodynamics: 'small' (ultraviolet) clusters of finite size in units of the lattice spacing a, and 'large' (infrared) clusters that percolate through the entire lattice independently of its size. The density of monopoles[2] belonging to the infrared clusters is subject to scaling, i.e., has a finite value in the continuum limit [24]. The distribution of clusters over size[3] for the full QCD is shown in Fig. 2a. One can see that the distribution of infrared clusters on a large lattice ($24^3 \times 48$) is separated by a gap from the distribution of ultraviolet clusters. On a smaller lattice ($16^3 \times 32$) there is no clear separation between the infrared and ultraviolet clusters (Fig. 2b).

Figure 3 presents the monopole density

$$\rho = \frac{1}{12V} \sum_{l, {}^*s, \mu} \left| k^{(l)}({}^*s, \mu) \right| \tag{22}$$

versus the ratio of the π- and ρ-meson masses. This ratio decreases with the quark mass.

The monopole density in the full QCD being larger than in gluodynamics can be qualitatively explained as follows. In Refs [25–27], monopoles have been shown to be correlated with instantons. On the other hand, the fermion determinant leads to attraction between instantons and anti-instantons, which increases as the quark mass decreases. This causes the production of instanton – anti-instanton pairs, the total number of instantons and of anti-instantons increases, and the monopole density must increase accordingly. And most of the additional monopole trajectories represent small closed paths around the instanton centers, which turns out to be important for the explanation of the monopole current asymmetry observed at a finite temperature (see Section 4.3).

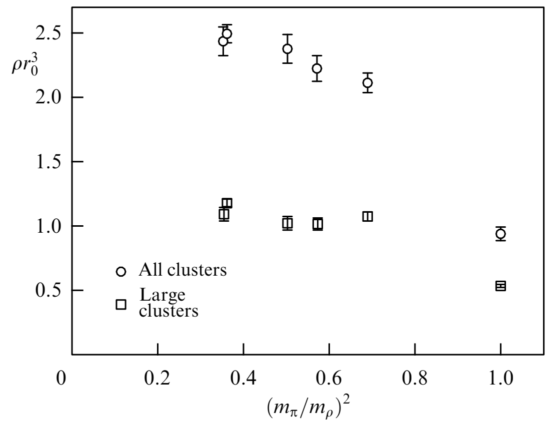

Figure 3. Monopole density in the full QCD; $m_\pi/m_\rho = 1$ corresponds to gluodynamics with $\beta = 6.0$.

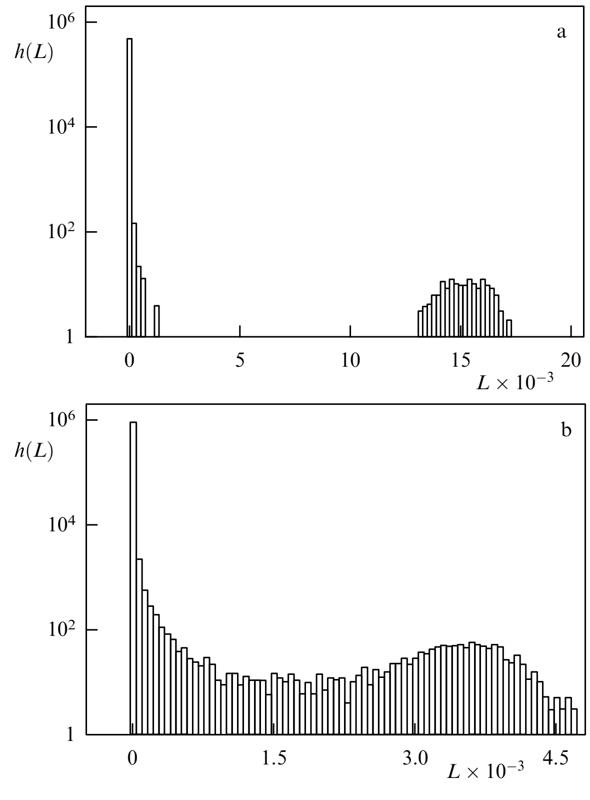

Figure 2. Distribution of monopole cluster lengths: (a) on the $24^3 \times 48$ lattice, $\beta = 5.29$, $\varkappa = 0.1355$; (b) on the $16^3 \times 32$ lattice, $\beta = 5.29$, $\varkappa = 0.135$.

3.4 Potential between heavy quarks

The principle of Abelian dominance [28] consists in the fact that in the Abelian projection the physical quantities related to the infrared properties of theory can be calculated with high precision with the aid of operators constructed only from Abelian variables, i.e., the averages $\langle \mathcal{O} \rangle^{\text{nonAb}}$ and $\langle \mathcal{O} \rangle^{\text{Ab}}$, namely

$$\langle \mathcal{O} \rangle^{\text{nonAb}} = \frac{1}{\mathcal{Z}} \int \exp(-\tilde{S}_{\text{eff}})\, \mathcal{O}(U_\mu)\, \mathcal{D}U_\mu(s)\,, \tag{23}$$

$$\langle \mathcal{O} \rangle^{\text{Ab}} = \frac{1}{\mathcal{Z}} \int \exp(-\tilde{S}_{\text{eff}})\, \mathcal{O}(u_\mu)\, \mathcal{D}U_\mu(s)\,, \tag{24}$$

yield values for physical quantities, determining the infrared behavior of the theory, which coincide with each other with good accuracy. An example of such a physical quantity is represented by the string tension. Thus, in calculating Abelian operators the link matrices $U_\mu(s)$ are replaced by the diagonal ones, $u_\mu(s)$. The action $\tilde{S}_{\text{eff}}$ represents the QCD action including the term fixing the gauge, and the logarithm of the Faddeev – Popov determinant. Integration in formulas (23) and (24) is performed over the 'fundamental modular region' in accordance with the procedure for fixing the gauge nonperturbatively [29]. Note that $\langle \mathcal{O} \rangle^{\text{Ab}}$ depends on the choice of Abelian gauge. At present, Abelian dominance has been confirmed for gluodynamics in the MA gauge defined in Section 3.3. In the present section we shall demonstrate the principle of Abelian (and monopole) dominance using the example of the static quark – antiquark interaction potential. The static potential is determined in the standard manner from the Wilson loop. For example, the Abelian potential is expressed in the form

$$V_{\text{ab}}(r) = \lim_{\mathcal{T} \to \infty} \frac{\langle W_{\text{ab}}(r, \mathcal{T}) \rangle}{\langle W_{\text{ab}}(r, \mathcal{T}+1) \rangle}\,, \tag{25}$$

[2] Concerning the monopole density, we apply the conventional terminology. QCD vacuum is magnetically neutral, and at each moment of time the number of monopoles equals the number of antimonopoles. In discussions of the monopole density it is the density of the monopole – antimonopole gas that is intended.

[3] The total length of the lines of magnetic currents, composing the given cluster, is called the size of the cluster.

where

$$W_{\mathrm{ab}}(r, \mathcal{T}) = \frac{1}{3}\,\mathrm{Tr}\,\mathcal{W}_{\mathcal{C}}\,,$$
$$\mathcal{W}_{\mathcal{C}} = \prod_{s\in\mathcal{C}} \mathrm{diag}\left(u_\mu^{(1)}(s), u_\mu^{(2)}(s), u_\mu^{(3)}(s)\right), \qquad (26)$$

and $\mathcal{C}$ is a contour of size $r \times \mathcal{T}$. In practice, the limit $\mathcal{T} \to \infty$ in expression (25) is achieved with difficulty, so a 'smearing' procedure is applied for the space-like link variables $u_\mu(s)$. This has permitted us to essentially improve the overlap integral of the wave function of the state created by our operator and the real wave function of the quark–antiquark pair and, already for $\mathcal{T}/a = 5$, to obtain the asymptotic value for the potential (25). The data for $V_{\mathrm{ab}}(r)$ were fitted by the function

$$V_{\mathrm{ab}}(r) = V_{\mathrm{ab}}^0 + \sigma_{\mathrm{ab}} r - \frac{\alpha_{\mathrm{ab}}}{r}\,, \qquad (27)$$

where σ_{ab} is the Abelian string tension, α_{ab} is the Abelian Coulomb coefficient, and V_{ab}^0 is the Abelian self-energy of the static sources.

Figures 4a,b show the static potential for SU(3) gluodynamics and for the full QCD. From Table 2 one can see that Abelian dominance is fulfilled with good accuracy.

For a more detailed investigation of the role of monopoles, the Abelian link variables can be decomposed into 'monopole' and 'photon' parts [30, 31]:

Table 2. Abelian and monopole tensions of a string and the monopole screening length in full QCD and in SU(3) gluodynamics.

m_π/m_ρ	$\sigma_{\mathrm{ab}}/\sigma$	$\sigma_{\mathrm{mon}}/\sigma_{\mathrm{ab}}$	ξ/r_0	$\sigma_{\mathrm{ab}}/\rho\xi$
0.6014 (96)	0.89 (4)	0.80 (4)	0.484 (19)	2.1 (2)
0.7095 (70)	0.95 (3)	0.87 (3)	0.466 (26)	2.6 (3)
0.7565 (44)	0.97 (6)	0.83 (8)	0.521 (17)	2.3 (2)
0.8306 (26)	0.97 (6)	0.88 (5)	0.482 (17)	2.5 (2)
—	0.83 (3)	0.84 (3)	0.662 (34)	3.2 (3)

$$\theta_\mu^{(l)}(s) = \theta_\mu^{(l)\,\mathrm{mon}}(s) + \theta_\mu^{(l)\,\mathrm{ph}}(s)\,, \qquad (28)$$

$$\theta_\mu^{(l)\,\mathrm{mon}}(s) = 2\pi \sum_{s'} D(s-s')\,\nabla_\alpha^- m_{\alpha\mu}^{(l)}(s')\,, \qquad (29)$$

where $D(s) = \Delta^{-1}(s)$ is the Coulomb propagator on the lattice, and $m_{\alpha\mu}^{(l)}(s')$ is the number of Dirac strings crossing the (s, α, μ) plaquette. The meaning of such a decomposition lies in the fact that the monopole current (18) is expressed only via $\theta_\mu^{(l)\,\mathrm{mon}}(s)$. From the monopole and photon fields, it is possible to extract the monopole and photon contributions to the Abelian potential. These contributions are presented in Figs 4c, d for gluodynamics and for the full QCD. It turns out that the monopole contribution provides for more than 80% of the Abelian string tension, while the photon part of the potential actually contributes nothing at all to σ. All these facts are in agreement with the monopole mechanism of color confinement.

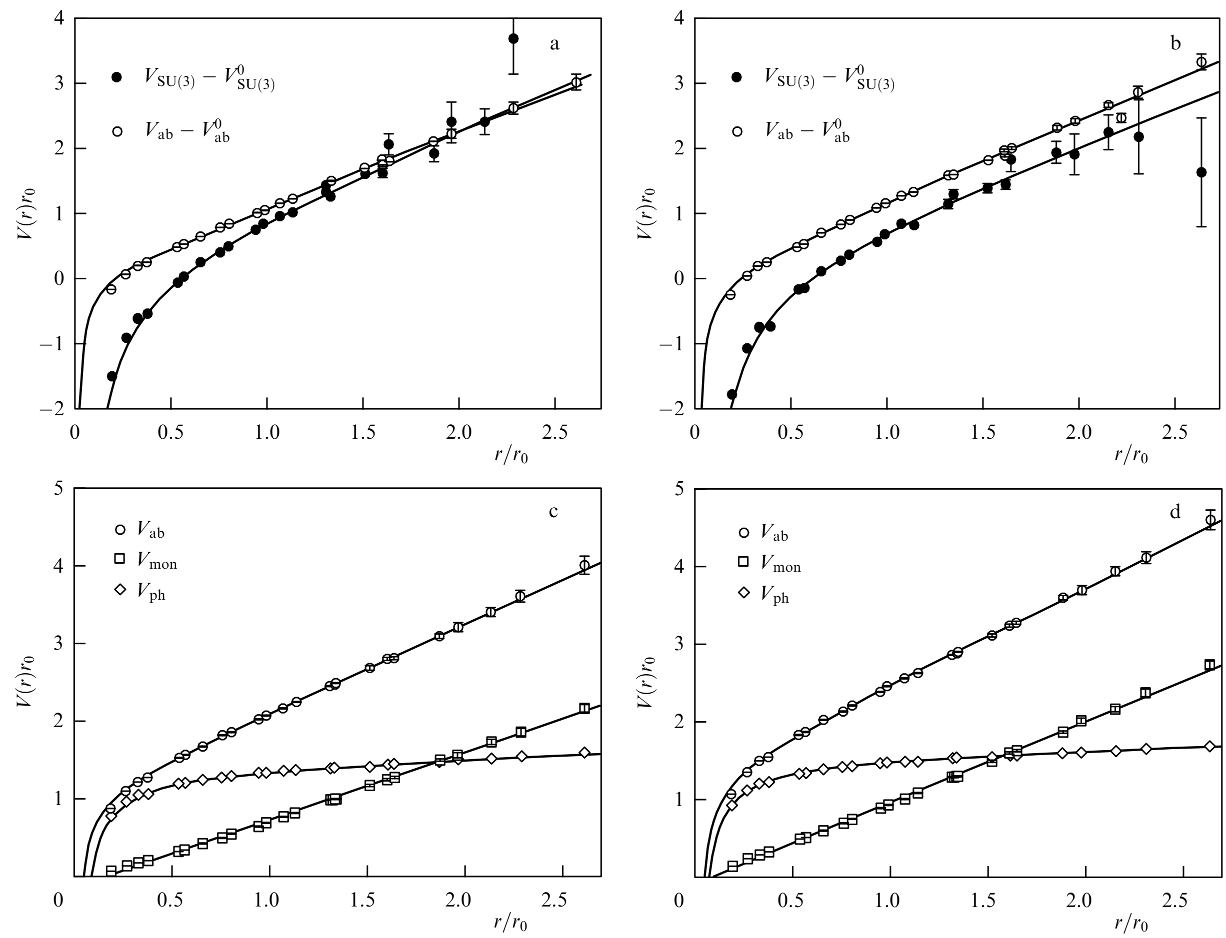

Figure 4. Total and Abelian static potentials: (a) for SU(3) gluodynamics ($\beta = 6.0$); (b) for the full QCD ($\beta = 5.29$, $\varkappa = 0.135$). Decomposition of the Abelian potential into the monopole and photon parts: (c) SU(3) gluodynamics, $\beta = 6.0$; (d) full QCD, $\beta = 5.29$, $\varkappa = 0.135$.

3.5 Screening of a magnetic charge

If the model of a vacuum as a dual superconductor is correct, then the monopole charge should be screened by the exponential $\exp(-r/\xi)$, where ξ is the inverse mass of the dual photon. Indeed, we observe such a screening by measuring the magnetic flux through a sphere of radius r surrounding a magnetic monopole. In a finite volume, the flux should not fall exponentially, but as

$$\Phi(r) = \Phi_0 \exp\left(-\frac{L}{2\xi}\right) \operatorname{sh} \frac{L-2r}{2\xi}\,, \tag{30}$$

where L is the lattice size. Fitting the parameters Φ_0 and ξ on the basis of numerical data yields the values for ξ given in Table 2. An example of fitting numerical data with the aid of expression (30) is shown in Fig. 5.

The dependence of ξ upon m_π/m_ρ enables us to explain qualitatively why the string tension remains practically intact in the full QCD, with a monopole density ρ exceeding the value obtained in gluodynamics. In the model of a monopole gas without interaction [23], one finds $\sigma \propto \rho\xi$. From Table 2 it follows that the density ρ increases with the ratio m_π/m_ρ, while the inverse dual-photon mass ξ decreases, which explains why the string tension does not change.

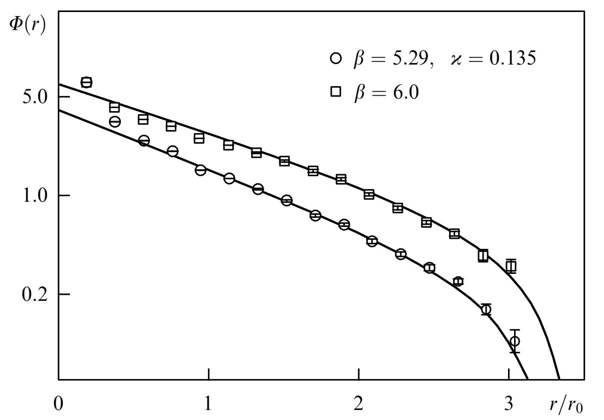

Figure 5. Fitting numerical data for the field flux of a magnetic charge.

3.6 Color string, observables

Investigation of the string between a quark and antiquark in SU(2) gluodynamics in the MA projection reveals that the monopole current and the electric field satisfy the dual Ampere law [32–34]. Moreover, they obey classical equations of motion for a dual superconductor (the dual Abelian Higgs model) [35]. In this section we present our results [1] which demonstrate the dual Ampere law to be obeyed for the averages $\langle \mathbf{E} \rangle$ and $\langle \mathbf{k} \rangle$ in the vicinity of a string providing color confinement in the full QCD, and describe the structure of this string in terms of Abelian variables.

To calculate the average magnitude of the Abelian operator

$$\mathcal{O}(s) = \operatorname{diag}\left[\mathcal{O}^{(1)}(s), \mathcal{O}^{(2)}(s), \mathcal{O}^{(3)}(s)\right] \tag{31}$$

in the field of a string, one computes the following correlators

$$\langle \mathcal{O}(s) \rangle_{\mathcal{W}} \equiv \frac{1}{3}\,\frac{\langle \operatorname{Tr} \mathcal{O}(s) \operatorname{Tr} \mathcal{W}_C \rangle}{\langle \operatorname{Tr} \mathcal{W}_C \rangle} - \frac{1}{3} \langle \operatorname{Tr}\, \mathcal{O} \rangle\,. \tag{32}$$

This expression holds valid for C-even operators such as the action density and the monopole density. In the case of C-odd operators, such as the electric field and the monopole current, averages of the following type are considered:

$$\langle \mathcal{O}(s) \rangle_{\mathcal{W}} \equiv \frac{\langle \operatorname{Tr}\,(\mathcal{O}(s)\, \mathcal{W}_C) \rangle}{\langle \operatorname{Tr} \mathcal{W}_C \rangle}\,. \tag{33}$$

In expressions (32) and (33), the Abelian Wilson loop $\mathcal{W}_C$ [see Eqn (26)] corresponds to a rectangular contour $r \times \mathcal{T}$. When the string profile is measured, the static quarks are fixed at points $x = 0$ and $x = r$. The operator $\mathcal{O}(s)$ is situated either in the xy, $z = 0$ plane, and $t = \mathcal{T}/2$, or in the xz, $y = 0$ plane, and $t = \mathcal{T}/2$. The distance from point s to the line connecting the static quarks will be denoted by $r_\perp$.

To calculate the action density ρ_A, one applies the operator

$$\mathcal{O}(s) = \frac{\beta}{3} \sum_{\mu > \nu} \operatorname{diag}\left[\cos\theta^{(1)}_{\mu\nu}(s),\ \cos\theta^{(2)}_{\mu\nu}(s),\ \cos\theta^{(3)}_{\mu\nu}(s)\right], \tag{34}$$

where $\theta^{(l)}_{\mu\nu}(s)$ are the Abelian plaquette angles constructed from the link angles $\theta^{(l)}_{\mu}(s)$ (16). Note that the action densities in Euclidean space and in Minkowski space are opposite in sign [32, 33].

The operator for calculation of the electric field is obtained from the plaquette angles $\theta^{(l)}_{\mu\nu}(s)$ precisely in the same way as for the SU(2) gauge group [33]:

$$\mathcal{O}_j(s) = \operatorname{diag}\left(\mathrm{i}\theta^{(1)}_{4j}(s),\, \mathrm{i}\theta^{(2)}_{4j}(s),\, \mathrm{i}\theta^{(3)}_{4j}(s)\right), \tag{35}$$

and the monopole current operator is defined by the expression

$$\mathcal{O}^{(l)}_j({}^*s) = 2\pi\mathrm{i} k^{(l)}({}^*s, \mu)\,. \tag{36}$$

The local monopole density $\rho({}^*s)$ is determined with the aid of the operator

$$\mathcal{O}({}^*s) = \frac{1}{4} \sum_{\mu} \operatorname{diag}\Big(\left|k^{(1)}({}^*s,\mu)\right|,\ \left|k^{(2)}({}^*s,\mu)\right|,\ \left|k^{(3)}({}^*s,\mu)\right|\Big). \tag{37}$$

3.7 Structure of an Abelian string

In this section we describe the structure of a string in full QCD and in SU(3) gluodynamics for a distance of about 1 fm between the probe quarks.

Figures 6a, b present the average action density corresponding to operator (34). Fitting the profile of the action density (Fig. 6c) with the function

$$\rho_A\left(r_\perp,\, x = \frac{r}{2}\right) = \text{const} \exp\left(-\frac{r_\perp^2}{\delta^2}\right) \tag{38}$$

yields the value $\delta = 0.29(1)$ fm both for QCD with dynamical quarks and for SU(3) gluodynamics.

Figures 7a, b depict the electric field of a string. One can readily see that within a narrow region around the axis connecting the quark and the antiquark, the field is directed along this axis, as expected for a string giving rise to color confinement. The profile of the longitudinal electric field component in an Abelian string is displayed in Fig. 7c. There exists a small difference in these profiles for SU(3)

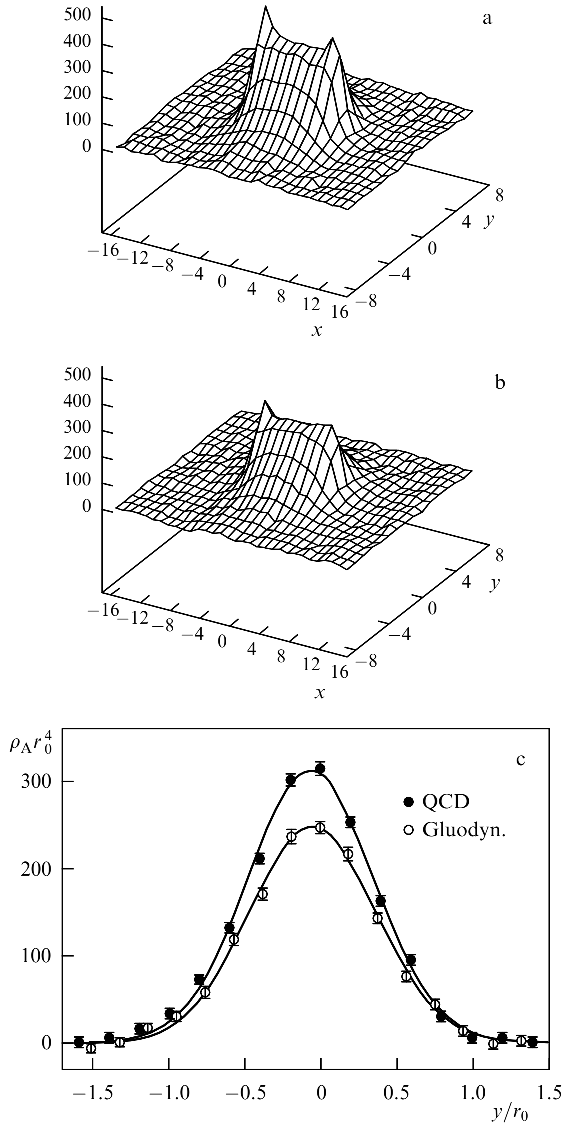

Figure 6. Action density $\rho_A(s)r_0^4$ of an Abelian string in full QCD (a) and in SU(3) gluodynamics (b), and the density profile at the center of the string for both theories (c).

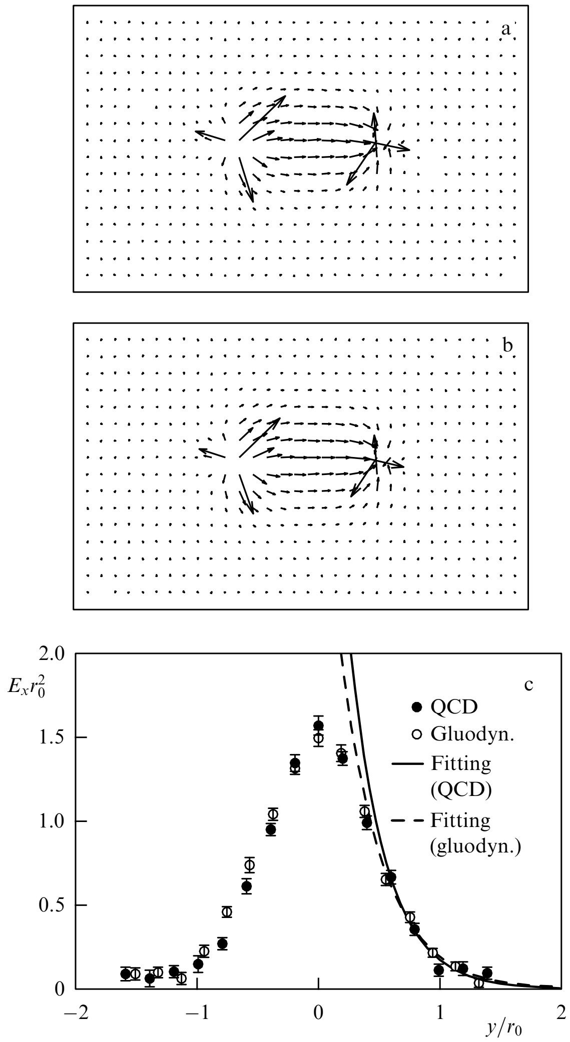

Figure 7. Electric field of a string in full QCD (a) and in SU(3) gluodynamics (b), and its profile at the center of the string for both theories (c).

gluodynamics and for QCD with dynamical quarks. Fitting the data for $r_\perp > 0.25$ fm with the function

$$E_x = \text{const} \exp\left(-\frac{r_\perp}{\lambda}\right) \tag{39}$$

yields the penetration depth $\lambda = 0.15(1)$ fm for full QCD, and $\lambda = 0.17(1)$ fm for SU(3) gluodynamics.

Figure 8 presents the monopole density corresponding to operator (37) in a string connecting the probe quark and antiquark. The monopole density outside the string is about twice as large in the case of QCD with dynamical quarks than in the case of SU(3) gluodynamics, which is in agreement with Fig. 3. At the center of the string, the monopole density is small in accordance with the monopole mechanism of color confinement: the Higgs field condensate is suppressed inside the Abrikosov – Nilsen – Olsen string. In this same model, the monopole current and the electric field should satisfy the dual Ampere law

$$\mathbf{k} = \nabla \times \mathbf{E}\,. \tag{40}$$

The monopole currents in the plane perpendicular to the string connecting the probe quark and antiquark are depicted in Figs 9a, b. It can be seen that the current twists around the center of the string, and only the current component perpendicular to the radius differs from zero. Figures 9c, d present the numerical data for the left-hand and right-hand parts of formula (40) inside the string produced by the probe quark and antiquark. From these figures we notice that the dual Ampere law works well both in the full QCD and in SU(3) gluodynamics. In the case of SU(2) gluodynamics, the dual Ampere law is obeyed with an even higher precision [33 – 35]. The fact itself that the dual Ampere law holds true inside the string responsible for confinement is essentially nontrivial. It is probably a consequence of Abelian fields in the gauge considered play an important part in the color confinement effect, and this phenomenon may serve as a starting point for developing the theory of confinement.

3.8 Long strings

If in full QCD the probe quark and antiquark are separated by a large distance, then the string in between them will disrupt, owing to the production of a quark – antiquark pair

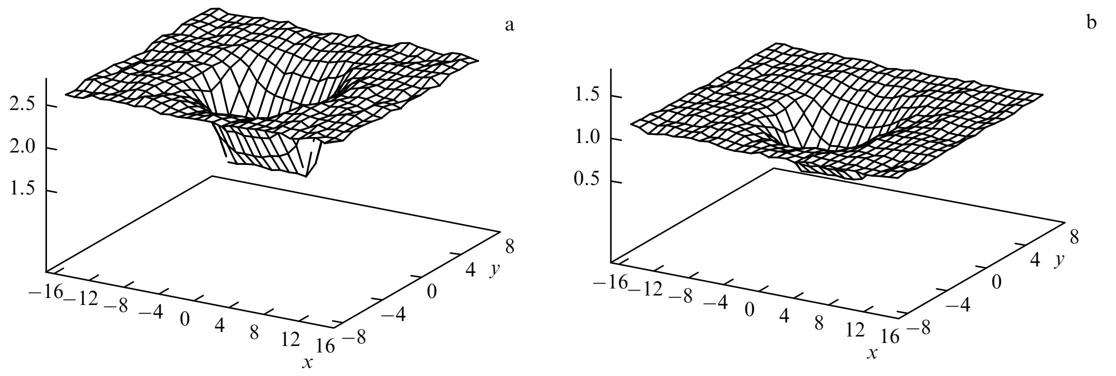

Figure 8. Monopole density $\rho(^*s)\, r_0^3$ in a string in full QCD (a), and in SU(3) gluodynamics (b).

from the vacuum. In the present review we consider virtual quarks of mass ~ 100 MeV, and in this case the distance at which the string is expected to disrupt is estimated at a level of 1.2 fm. Figure 10 shows the electric field of a string on a $24^3 \times 48$ lattice for $r/a = 18$, which corresponds to a string length of 1.6 fm. To reduce the statistical noise, the electric field was extracted from the monopole part of the link variables. In spite of the large length of the string, no signs of its breaking are seen. A possible explanation of this fact is the following [36–40]. The state created by the operator of the Wilson loop overlaps very little with the state corresponding to a broken string; the contribution of the latter state is significant only for such $\mathcal{T}$ that satisfy the inequality $\exp\big(-2m_{\mathrm{SL}}(r+\mathcal{T})\big) \gg \exp(-\sigma r \mathcal{T})$, where m_{SL} is the energy of the meson produced by a sea quark and the test static quark, without considering the self-energy of a static quark. This estimation gives $\mathcal{T} \gg 3$ fm for $r \approx 1.5$ fm [38]. In lattice units $\mathcal{T} = 3$ fm corresponds to $\mathcal{T}/a = 34$, but we could not take more than $\mathcal{T}/a = 10$, owing to the rapidly decreasing signal-to-noise ratio. Thus, observation of the breaking of a string on a lattice turns out to be a very difficult task. However, in Section 4.2 it will be shown that at a finite temperature (but below the phase transition temperature, i.e., in the confinement phase) string breaking can actually be seen in the results of numerical simulations.

Fitting the action density profile of a long string with the aid of formula (38) yields $\delta = 0.30(3)$ fm; approximately the same width was obtained, also, for $r = 1$ fm. This is quite a surprising result, since string models with the effective Nambu–Goto action predict broadening of the string as the

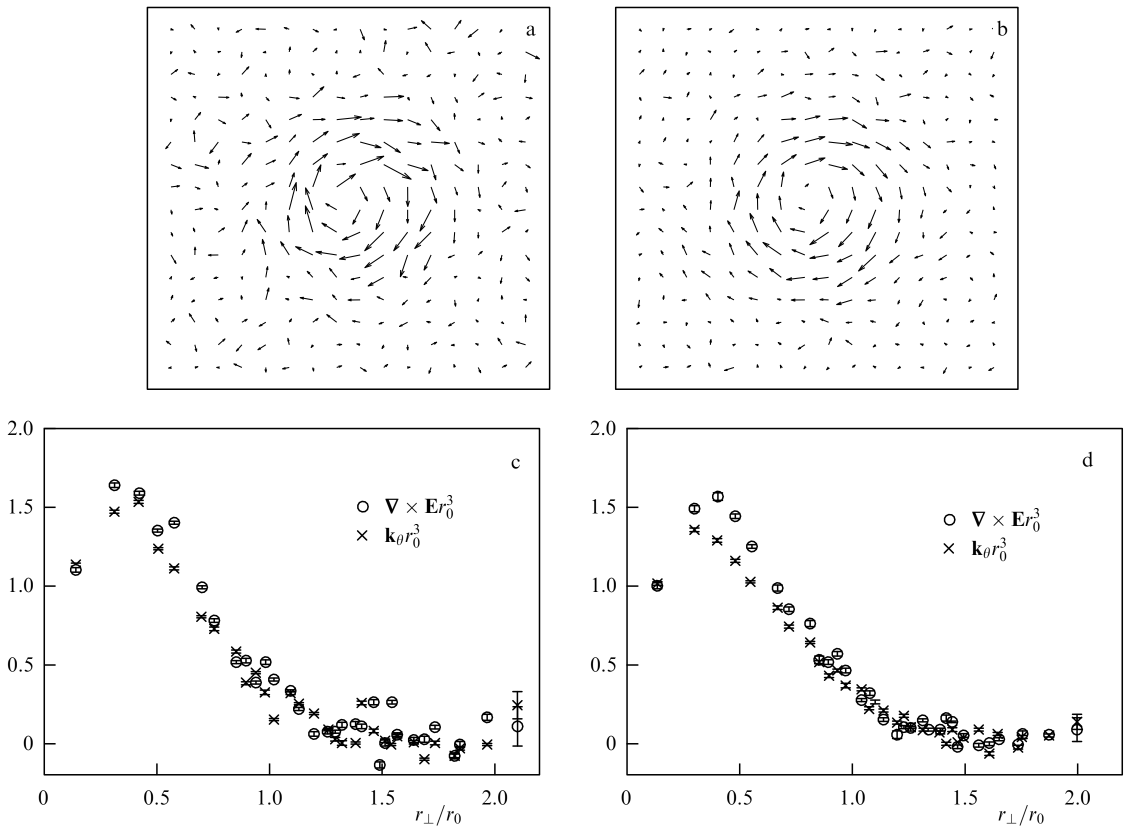

Figure 9. Monopole current $\mathbf{k} r_0^3$ at the center of a string ($x = r/2$) in full QCD (a), and in SU(3) gluodynamics (b). Verification of the dual Ampere law in full QCD (c), and in SU(3) gluodynamics (d).

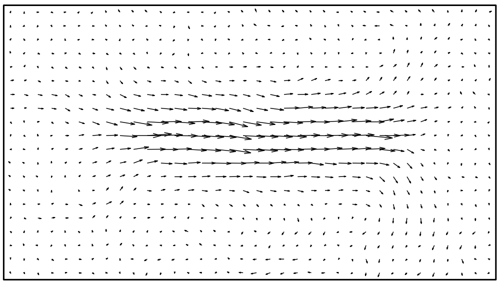

Figure 10. Monopole part of the electric field of a string, obtained on $24^3 \times 48$ lattice for the Wilson loop on a contour $r \approx 1.6$ fm, $\mathcal{T} \approx 0.9$ fm.

distance r increases [41]. We note that no string broadening was also found in SU(2) gluodynamics [42].

4. Finite temperatures

An increase in temperature in SU(3) gluodynamics results in a first-order phase transition which separates the color charge confinement phase (low temperatures) and the free-color phase. In this model, the order parameter of the phase transition at finite temperatures is the fundamental Polyakov loop which is defined as the product of link variables U_4 along the straight path closed due to the boundary conditions:

$$L(\mathbf{x}) = \prod_{t=1}^{L_t} U_4(\mathbf{x}, t)\,. \tag{41}$$

The nonzero value of an average Polyakov loop, observed in the high-temperature phase, points to global Z(3) symmetry breaking. The Polyakov loop serves as an order parameter only for the model without dynamical quarks, i.e., in the case of infinitely large quark masses. In the opposite limit of zero quark masses (i.e., in the QCD chiral limit), it is the chiral condensate $\langle\bar{\psi}\psi\rangle$ that serves as the order parameter. The order of the phase transition depends on the number of massless quarks: the chiral phase transition in QCD with three massless quarks is a first-order transition, while in the case of two quarks no phase transition occurs and, instead of a phase transition, one observes a so-called soft crossover (often termed a 'continuum phase transition'). The properties of a phase transition in real QCD are determined by two light (u and d) and one heavier (s) quarks, while the remaining quarks are too heavy to exert a noticeable influence. In the case of nonzero and finite quark masses, neither the Polyakov loop nor the chiral condensate are, strictly speaking, the order parameters. Numerical results, however, show that the susceptibilities of both order parameters can be used for determining the transition point [43]. In Sections 4.1–4.3, we shall deal with the numerical results for the critical temperature, the parameters of the static interquark potential, and the properties of monopoles at finite temperatures, obtained by us in Refs [2, 3].

4.1 Critical temperature

One of the simplest operators describing color confinement-deconfinement transition is the average Polyakov loop (41). As already discussed at the beginning of Section 4, the quantum average of this operator is not a rigorous order operator but, nevertheless, this quantity presents a certain interest. The quantum averages for various types of Polyakov loops are shown in Fig. 11a.

The non-Abelian Polyakov loop $\langle L\rangle$, as well as the Abelian, monopole, and photon components presented in Fig. 11a, are seen to exhibit no jumps. The Polyakov loops are small in the deconfinement phase (small $\varkappa$) and gradually increase with the parameter $\varkappa$, which corresponds to penetration into the depths of deconfinement phase. The contribution of photons to the Polyakov loop is practically insensitive to the phase transition, contrary to the Abelian and monopole contributions. It may also be noted that in the case of QCD, like in the theory without fields of matter, the monopole and photon contributions to the Abelian loop factorize: $\langle L_{\text{Ab}}\rangle \approx \langle L_{\text{mon}}\rangle\langle L_{\text{ph}}\rangle$. These properties of the Polyakov loop averages indicate that precisely monopole degrees of freedom are essential (i.e., precisely these degrees of freedom carry nonperturbative information) for a phase transition, while the photon degree of freedom is totally perturbative.

The next step consists in determination of the critical value of the parameter $\varkappa$ (further denoted by $\varkappa_c$). The simplest method for finding $\varkappa_c$ consists in determining the maximum numerical value of the Polyakov loop susceptibility χ, where it is correctly reasoned that $\chi \sim \langle L^2\rangle - \langle L\rangle^2$. In the non-Abelian case, $\varkappa_c = 0.1344(1)$ at $\beta = 5.2$, and $\varkappa_c = 0.1341(1)$

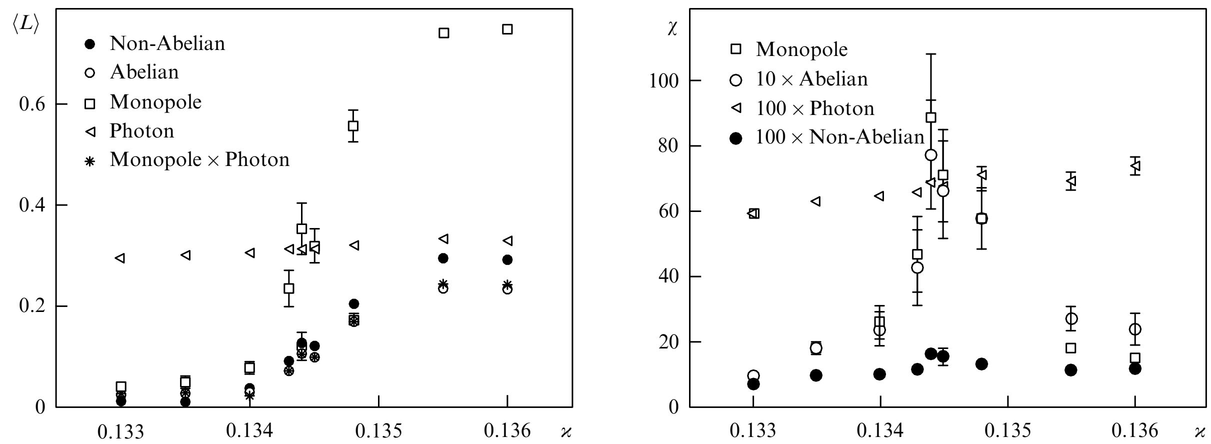

Figure 11. (a) The non-Abelian, Abelian, and monopole Polyakov loop averages, as well as the product of the monopole and photon loop averages; (b) the respective susceptibilities for $\beta = 5.2$.

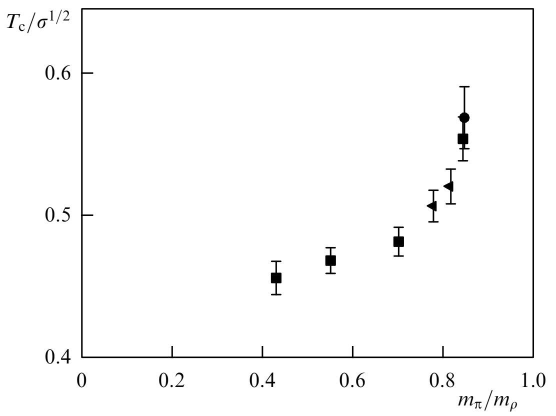

Figure 12. Critical temperature of the phase transition. The data presented by triangles were obtained in Ref. [2], by squares in Ref. [45], and by the circle in Ref. [46].

for $\beta = 5.25$, according to Fig. 11b. The critical values of the parameter $\varkappa$ correspond to certain critical temperatures which can be obtained with the aid of the interpolation formula presented in Ref. [44]: $T_c r_0 = 0.54(2)$ for $\beta = 5.2$, and $T_c r_0 = 0.56(2)$ for $\beta = 5.25$. For estimation of the temperature in physical units, one can use the value of $1/r_0 = 394$ MeV, for which one obtains $T_c = 213(10)$ MeV and $T_c = 222(10)$ MeV at $\beta = 5.2$ and $\beta = 5.25$, respectively. By determining the ratio between the meson masses at these critical points [44], $m_\pi/m_\rho = 0.78$ and 0.82, it is possible to derive the dependence of the critical temperature upon m_π/m_ρ.

In Figure 12, our results for the transition temperature, determined by the maximum of susceptibility, are presented together with the results of Refs [45] and [46]. For calculation of the ratio $T_c/\sqrt{\sigma}$, the phenomenological value $\sqrt{\sigma} = 425$ MeV was employed. From the figure one can see that the results of all groups are in good agreement with each other. We note that the calculations presented in Refs [45] and [46] were performed with another (larger) lattice spacing. Therefore, from Fig. 12 it follows that the critical temperature is practically independent of the lattice spacing. The Abelian, monopole, and photon susceptibilities are given in Fig. 11b (for one value of the lattice coupling constant $\beta = 5.2$). It can be emphasized that the Abelian and monopole susceptibilities exhibit a maximum at one and the same value of the parameter $\varkappa$, which, in turn, coincides with the peak of non-Abelian susceptibility, also shown in Fig. 11b. We point out that the monopole susceptibility exceeds the Abelian one by an order of magnitude, while the Abelian susceptibility is much larger than the non-Abelian one (the difference, here, is also approximately one order of magnitude). The photon susceptibility remains practically intact at the critical temperature, as was to be expected. These results once again confirm the fact that the monopole degrees of freedom are the ones most sensitive to phase transition.

4.2 Potential between heavy quarks at a finite temperature

The most evident effect due to accounting for dynamical quarks consists of the breaking of a chromodynamical string stretched between a quark and antiquark, if they are at a sufficiently large distance from each other. One of the most serious problems in studies of string breaking at zero temperature is the small overlap of the 'broken' state and the state created by the Wilson loop, as already discussed in Section 3.8. The situation is totally different at a nonzero temperature, when the Polyakov loops can be utilized for measuring the potential. In this case, the overlap of the 'broken' state and the state produced by the correlator of Polyakov loops is on the order of unity, which permits us to explicitly see the effect due to the breaking of the string. The potential $V(r,T)$ between the heavy (static) quarks is determined with the aid of the correlator of Polyakov loops as follows:

$$V(r,T) = -\ln\left\langle \frac{1}{9}\, L_{\mathbf{x}} L_{\mathbf{y}}^{\dagger} \right\rangle + C\,, \tag{42}$$

where the constant C includes the self-energy of static quarks and an entropy contribution. At sufficiently large distances, the correlator of Polyakov loops factorizes, so that

$$\langle L_{\mathbf{x}} L_{\mathbf{y}}^{\dagger}\rangle \to \left|\langle L\rangle\right|^2, \quad |\mathbf{x}-\mathbf{y}| \to \infty\,, \tag{43}$$

and $|\langle L\rangle|^2 \neq 0$, since the global $Z(3)$ symmetry is broken owing to the presence of dynamical fermions. It should be emphasized that the potential in expression (42) is a potential averaged over color. It is related to the singlet and octet potentials by the relationship [47]

$$\exp\left[-\frac{V(r,T)}{T}\right] = \frac{1}{9}\,\exp\left[-\frac{V_{\mathrm{sing}}(r,T)}{T}\right] + \frac{8}{9}\,\exp\left[-\frac{V_{\mathrm{oct}}(r,T)}{T}\right].$$

String breaking at nonzero temperature $T > 0$ in the QCD low-temperature phase was studied by DeTar et al. [48]. While discussing the interquark potential, it is appropriate to examine the spectral representation for the correlator of Polyakov loops [49]:

$$\langle L_{\mathbf{x}} L_{\mathbf{y}}^{\dagger}\rangle = \sum_{n=0}^{\infty} w_n \exp\left[-\frac{E_n(r)}{T}\right]. \tag{44}$$

As $T \to 0$, we can see that only the lowest state contributes to the potential, $V(r,0) = E_0(r)$ (with an accuracy up to a certain constant). On the contrary, the potential $V(r,T)$ for $T > 0$ includes contributions from all sorts of states.

At zero temperature, the singlet potential can be described by the string model only up to a certain distance R_{br} between the static quarks. At distances exceeding R_{br}, the string state is no longer the ground state, and it is substituted by the so-called 'broken string state' or, in other words, by the state of a pair of mesons composed of a heavy and a light (anti)quark. Thus, at low temperatures only two states in the spectrum are significant, and each of them serves as the ground state at certain distances. We have suggested [2] that at all temperatures below the critical temperature the correlator of Polyakov loops can be described with good precision with the aid of these two states — the string state and the two-meson state. In the calculations performed in Ref. [2], the singlet part of the potential was not singled out, i.e., the contribution of the octet potential was considered to be negligible.

Thus, we consider a two-exponential form for the correlator of Polyakov loops, namely

$$\frac{1}{9}\langle L_{\mathbf{x}} L_{\mathbf{y}}^{\dagger}\rangle = \exp\left[-\frac{V_0 + V_{\mathrm{str}}(r,T)}{T}\right] + \exp\left[-\frac{2E(T)}{T}\right], \tag{45}$$

where the string potential $V_{\rm str}$ is represented in the form

$$V_{\rm str}(r,T) = -\frac{1}{r}\left[\alpha - \frac{1}{6}\arctan(2rT)\right] + \left[\sigma(T) + \frac{2T^2}{3}\arctan\frac{1}{2rT}\right] r + \frac{T}{2}\ln(1+4r^2T^2)\,. \quad (46)$$

Expression (46) was derived by Gao [50]. The string potential (46) includes the contributions from fluctuations of the chromodynamical string (the Casimir energy) stretched on static quark trajectories at a finite temperature T. In this case, the coefficient α is fixed: $\alpha = \pi/12$. However, this form of potential does not take into account ordinary Coulomb interaction which may modify the first term in the right-hand side of equation (46). Therefore, by analogy with Ref. [51], we have considered another value of this parameter, namely, $\alpha = 0.33$. As to the effective quark mass $m(T)$, it is determined by the exponent of the second term in the right-hand side of equation (45) after subtraction of the self-interaction energy:

$$m(T) = E(T) - \frac{V_0}{2}\,. \quad (47)$$

Our numerical calculations have shown that the static potential between a quark and an antiquark may be quite accurately described by the two-exponential formulas (45), (46). Examples of fittings are presented in Fig. 13a for $T/T_{\rm c} = 0.87$ and 0.98 (here, data were used for $\beta = 5.2$). Also presented in this figure is the asymptotic value of the potential $V_{\rm inf} = -2T\ln\langle L\rangle$. The potential is seen to tend toward its asymptotic value at maximum achievable values of the interquark distance.

The string tension and the effective quark mass obtained by fitting the non-Abelian potential are presented in Figs 14a, b. The string tension for gluodynamics [52] is shown by the shaded region. From these figures we notice that the values of the ratio $\sigma(T)/\sigma(0)$ in the theory with dynamical fermions lie somewhat higher than the respective values in the theory without fermions; however, the final conclusion on the relation between these quantities cannot be drawn yet owing to the quite large statistical and systematic uncertainties in our findings. Our values of the effective quark mass are higher than those obtained by Digal et al. [53] on the basis of numerical results taken from Ref. [43]. This distinction is, probably, explained by QCD with three flavors having been studied in Ref. [53], while we consider the theory with two flavors.

Having determined the parameters of the potential, we can calculate the distance $R_{\rm br}$ at which the chromodynamical string breaks. The distance $R_{\rm br}$ is determined by the equality between the first and second terms in the right-hand side of equation (45):

$$V_{\rm str}(R_{\rm br}, T) = 2m(T)\,. \quad (48)$$

This relation is illustrated in Fig. 13b, in which the energies are given of the string and of the two-meson states. The distance at which the energy levels intersect corresponds to $R_{\rm br}$.

The dependence of the distance $R_{\rm br}$ upon temperature is depicted in Fig. 14c. This distance decreases as the temperature increases, but at the critical temperature $T = T_{\rm c}$ the distance $R_{\rm br}$ does not equal zero.

4.3 Monopole dynamics

One of the most important characteristics of monopoles is the average density ρ of monopole trajectories, determined by equation (22). Figure 15a shows the monopole density for pure gluodynamics and for QCD. The data for pure gluodynamics were obtained on a lattice of the same size as that for the theory with fermions. As can be seen from Fig. 15a, the monopole density in the theory with dynamical fermions is significantly higher than in the theory without fermions, which is in agreement with the findings at zero temperature.

Another interesting characteristic of monopoles consists in the asymmetry of monopole currents, which is determined as follows:

$$\eta = \frac{\rho_t - \rho_s}{\rho_t + \rho_s}\,, \quad (49)$$

where ρ_t and ρ_s are the densities of the time and space magnetic currents, respectively:

$$\rho_t = \frac{1}{3N_t N_s^3}\left\langle \sum_{a=1}^{3}\sum_s \left|k_4^a(s)\right| \right\rangle,$$
$$\rho_s = \frac{1}{9N_t N_s^3}\left\langle \sum_{a=1}^{3}\sum_s\sum_{i=1}^{3} \left|k_i^a(s)\right| \right\rangle. \quad (50)$$

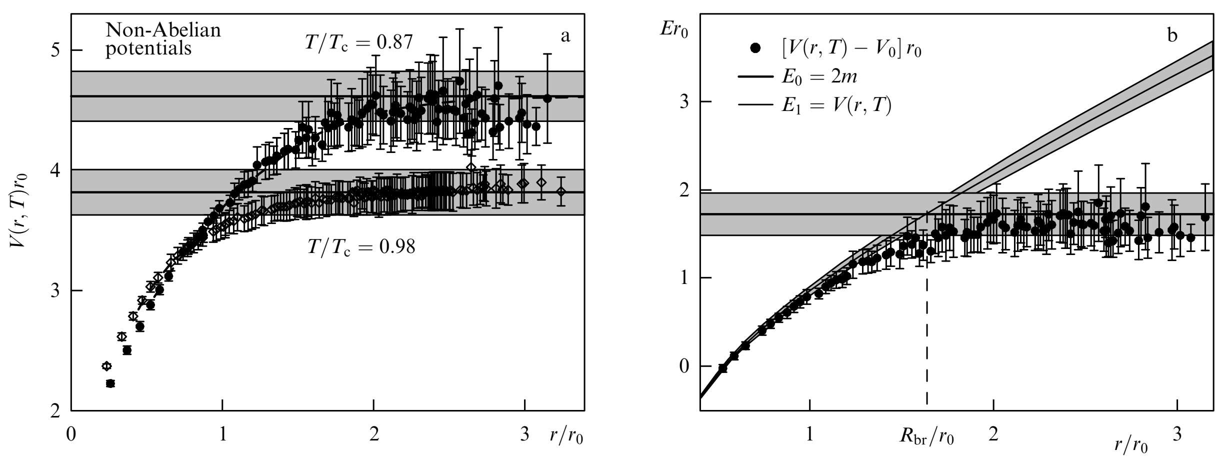

Figure 13. (a) Interquark potential with fitting curves for $T/T_{\rm c} = 0.87$ and 0.98, and the respective values of $V_{\rm inf}$; (b) energies of the string and two-meson states and $V_{\rm inf}$ for $T/T_{\rm c} = 0.87$.

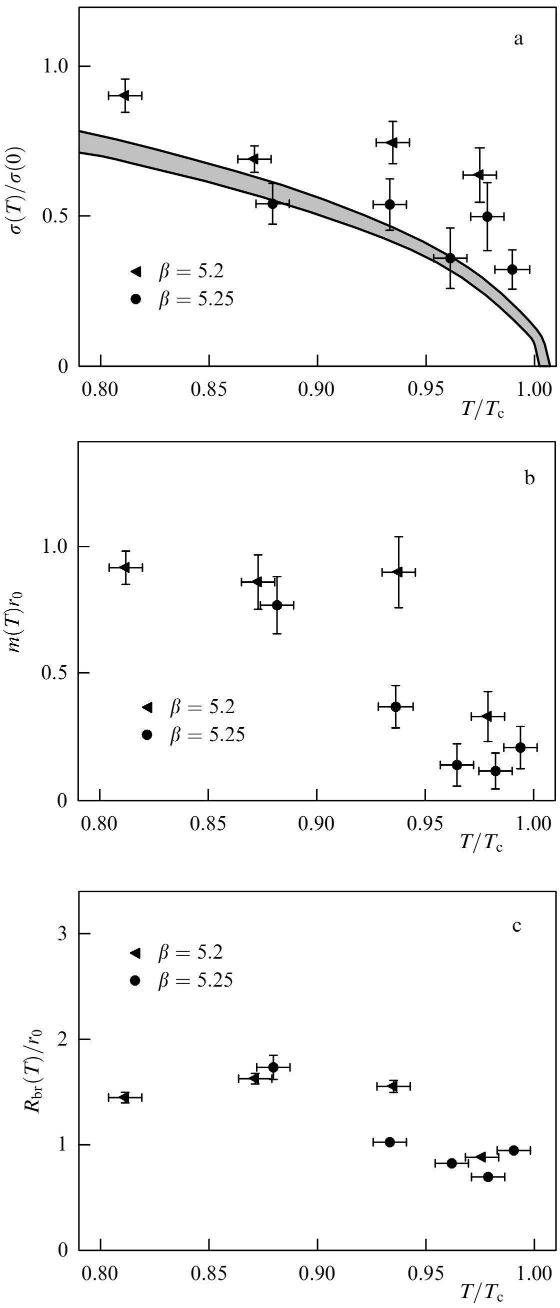

Figure 14. Plots of string tension (a), effective quark mass (b), and distance R_{br} between static quarks at which the string stretched between them breaks (c) versus temperature.

The meaning of the quantity η is rather simple: if all the currents are static, then $\eta = 1$, while if the monopole distribution is isotropic, then monopole currents exhibit no asymmetry and $\eta = 0$. It turns out that in the theory with fermions the asymmetry η equals zero in the color confinement phase, and it becomes nonzero above the critical point (Fig. 15b). A similar behavior of η is also observed in gluodynamics, where the monopoles become static in the limit of high temperatures. It should be emphasized, however, that the enhancement of η with temperature proceeds significantly more slowly in QCD than in gluodynamics.

The high monopole density in QCD and the asymmetry properties of monopole currents can be explained by the production of strong local quantum fluctuations in a vacuum due to the presence of the fermion determinant. Such fluctuations result in the formation of monopole loops (trajectories), while their local nature renders the loops short. The latter property results in symmetry between the space and time components of the monopole current in these monopole loops, since their size is small as compared with the inverse temperature (i.e., the size of the lattice in the time direction). Thus, the total monopole density turns out to be higher in QCD than in gluodynamics. Here, owing to the isotropy of short monopole loops, the difference $\rho_t - \rho_s$ varies to a lesser degree than the sum $\rho_t + \rho_s$, which is in accordance with the smaller asymmetry η in QCD as compared with its values in gluodynamics.

Another reason for the high monopole density in QCD may lie in the production of instanton – anti-instanton pairs. This phenomenon has already been discussed at the end of Section 3.3.

5. Investigation of baryon structure

In this section, string structure in a system of three static quarks at zero and nonzero temperatures is discussed. Investigation into the system of three static quarks on a lattice is important for obtaining information on the baryon structure. Until recently there was no answer to the question of whether true three-particle interaction (corresponding to the Y-like configuration of gluon fields) exists, or the interaction at large distances is the sum of two-particle interactions (Δ-shaped string) [55 – 59]. Certain lattice results were interpreted in favor of the Δ-configuration [56, 57], while, at the same time, other results supported the Y-shape hypothesis [58, 59]. Such a contradiction has existed for a long time owing to the difference between the predictions of these two hypotheses for the baryon potential being quite small, while high-precision lattice calculations are rendered difficult because of the rapid increase in the potential with the distance between the quarks. Therefore, it seems expedient to measure the gluon field distribution inside the baryon directly. It must be noted that not long ago the results were obtained for the baryon potential and the field distribution inside the baryon in the dual Abelian Higgs model as a model of a QCD vacuum [60, 61] and with the aid of the method of field correlators [62]. These findings point to the Y-like configuration of gluon fields.

5.1 Observables

We have studied the configuration of Abelian gluon fields in a three-quark system after fixing the MA gauge [4]. Utilizing Abelian variables reduces the statistical errors significantly, and since the investigation of the meson configuration has confirmed the existence of Abelian dominance after the MA gauge is fixed (see Section 3), one can count on the results, discussed in this section and obtained with Abelian operators, to correctly describe a non-Abelian baryon string. Our aim also includes comparison of the results obtained on a lattice with the predictions of the Landau – Ginzburg dual model [60, 61].

The translation of a baryon from point A to point B is described by the operator (the baryon Wilson loop [57, 59])

$$W_{3q} = \frac{1}{3!}\,\varepsilon^{ijk}\varepsilon^{i'j'k'}\,U_{\Gamma_1}^{ii'}U_{\Gamma_2}^{jj'}U_{\Gamma_3}^{kk'}\,, \qquad (51)$$

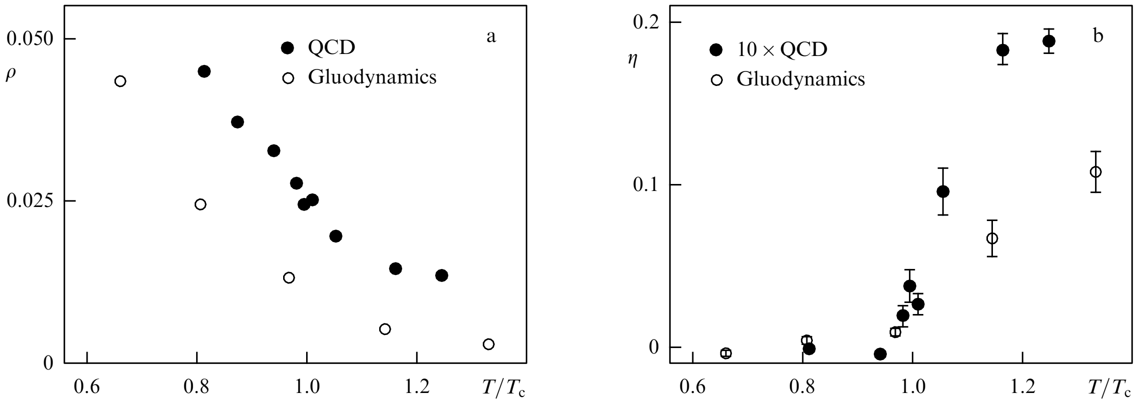

Figure 15. Plots of monopole density (a) and asymmetry of monopole currents (b) versus temperature.

where $U_\Gamma = \prod_{l \in \Gamma} U_l$ is the product of link matrices along the path Γ, and the trajectories of (infinitely heavy) quarks, connecting points A and B (Fig. 16a), are denoted by Γ_k.

The energy of the ground state of a baryon (the overall interaction potential of three quarks) is given by

$$V(x_1, x_2, x_3) = -\frac{1}{T} \lim_{T \to \infty} W_{3q} \,. \tag{52}$$

The Abelian baryon Wilson loop is expressed via the Abelian link variables $u_\mu(s)$, so that

$$W_{3q}^{\mathrm{Ab}} = \frac{1}{3!} \left|\varepsilon^{ijk}\right| u_{\Gamma_1}^{(i)} u_{\Gamma_2}^{(j)} u_{\Gamma_3}^{(k)} \,, \tag{53}$$

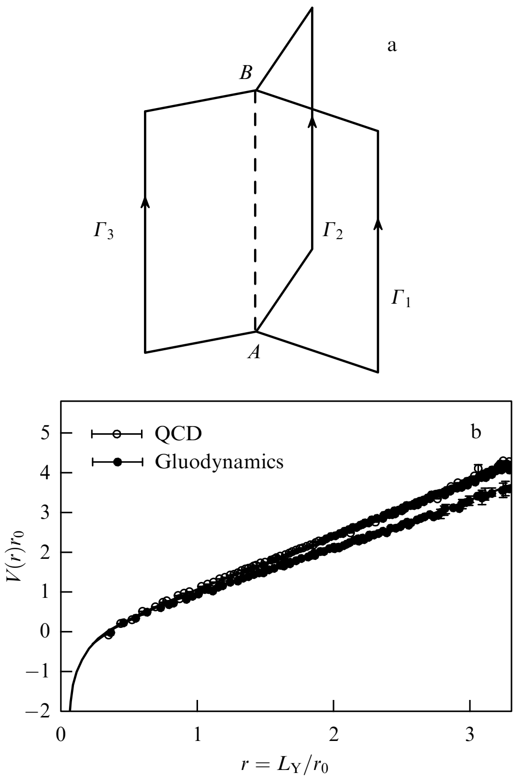

Figure 16. (a) Baryon Wilson loop; (b) comparison of the non-Abelian and Abelian baryon potentials calculated in gluodynamics.

by analogy with the non-Abelian loop (51). Local observables describing the baryon string are defined as the averages of the respective operators in the presence of the Wilson loop, which is similar to their definition in the case of the quark–antiquark system. For C-even observables, such as the action density, the averages are defined precisely in the same way by substitution of the baryon loop for the ordinary Wilson loop. In the case of C-odd observables, for example, the electric field, the average is determined as follows [4]:

$$\left\langle \mathcal{O}(s) \right\rangle_{3q} = \frac{\left\langle (1/3!) |\varepsilon_{ijk}| \mathcal{O}^{(i)}(s) u_{\Gamma_1}^{(i)} u_{\Gamma_2}^{(j)} u_{\Gamma_3}^{(k)} \right\rangle}{\left\langle W_{3q}^{\mathrm{Ab}} \right\rangle} \,. \tag{54}$$

At nonzero temperature, the product of three Polyakov loops is used, instead of the Wilson loop:

$$P_{3q}^{\mathrm{Ab}} = \frac{1}{3!} \left|\varepsilon^{ijk}\right| u_4^{(i)}(\mathbf{x}_1)\, u_4^{(j)}(\mathbf{x}_2)\, u_4^{(k)}(\mathbf{x}_3) \,, \tag{55}$$

where

$$u_4^{(i)}(\mathbf{x}_k) = \prod_{t=1}^{T} u_4^{(i)}(t, \mathbf{x}_k) \tag{56}$$

is an Abelian Polyakov loop. The averages, undergoing substitution of P_{3q}^{Ab} for W_{3q}^{Ab}, are determined just like in the case of zero temperature.

5.2 Static potential and string structure in a three-quark system at zero temperature

Figure 16b demonstrates the baryon potential as a function of L_Y — the minimum length of a baryon string exhibiting the Y-shape [59]. The solid curve corresponds to the potential fitted with the use of data for a configuration with equal distances between the quarks. In the case of such configurations, one has $|r_i - r_j| = L_Y/\sqrt{3}$ for all pairs i, j of quarks, and it is possible to apply a function of the following form for fitting:

$$V(L_Y) = -\frac{3\sqrt{3}e}{L_Y} - \sigma L_Y + V_0 \,. \tag{57}$$

The fitting yields the value 0.038(1) (in lattice units) for the Abelian string tension, which amounts to 83(3)% of the non-Abelian string tension [59]. This result points to the existence of Abelian dominance in the baryon system. It is expected

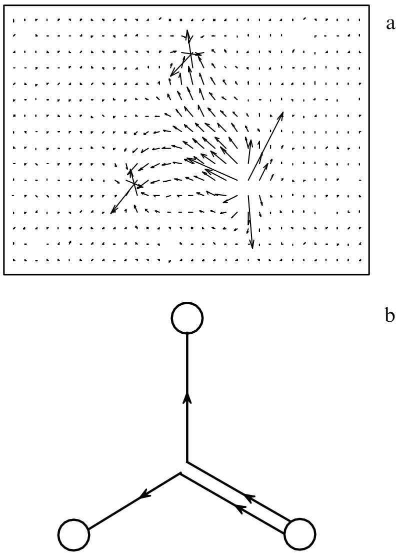

Figure 17. (a) Color electric field, and (b) its schematic image.

that the ratio between the Abelian and non-Abelian string tensions increases in the continuum limit, since such an enhancement has been revealed in SU(2) gluodynamics [63]. By performing a similar analysis for the full QCD we obtained the value 0.039(1) for the Abelian string tension, which coincides, within the limits of statistical error, with the result obtained in SU(3) gluodynamics.

Figure 17a shows the Abelian electric field in a three-quark system. The color index of the electric field operator in equation (54) coincides with the color index of the quark situated at the right bottom of Fig. 17a. This quark is clearly the source of color electric field flux. The flux is divided into two equal parts at the center of the baryon, each of which is absorbed by the other two quarks. The behavior of the electric field flux is presented schematically in Fig. 17b. The monopole and photon components of the Abelian potential are presented in Fig. 18. From this figure it follows that the monopole part of the Abelian gluon field is responsible for the linear potential, as in the case of quark – antiquark interaction.

The Abelian action density in the full QCD model is given in Fig. 19a. Three peaks corresponding to the positions of the

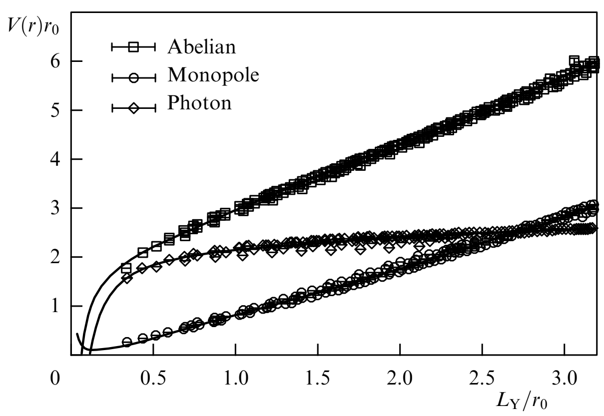

Figure 18. The Abelian baryon potential in the full QCD and its monopole and photon components as functions of L_Y.

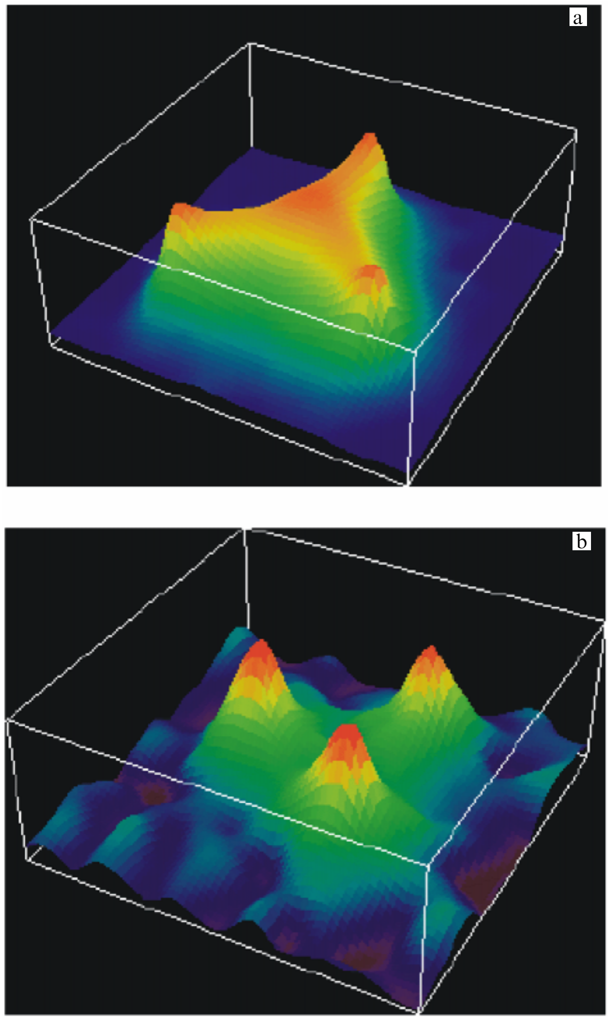

Figure 19. Abelian action density in a three-quark system in full QCD at $T = 0$ (a), and at $T = 1.25\,T_c$ (b)

static quarks and the string indicating color confinement can be noticed in the Abelian density. An important observation is the fact that at the center of the configuration there is a clear peak, which points to the Y-shape of the baryon string. In the photon component of the Abelian action density only peaks corresponding to sources are seen, while the monopole component fully reproduces the structure of the baryon string, including the peak at the center.

A similar picture is also observed in Fig. 20a, where the Abelian electric field and the corresponding monopole and photon components are depicted. The photon part is in qualitative agreement with the Coulomb field, while the monopole part shows no traces of sources. From Fig. 20b it can be noticed that in the plane perpendicular to the flux there exists a solenoidal magnetic current. Thus, the same scenario of color confinement is observed in a three-quark system as in a quark – antiquark pair [3]. Namely, the Coulomb field of sources induces in the QCD vacuum a solenoidal magnetic current. This current, in turn, induces an electric field having the shape of a string with Y-geometry and reducing the Coulomb field of sources in the space region outside the string. The results obtained are in agreement with the predictions of QCD vacuum properties following from the Landau – Ginzburg dual model [60, 61, 64].

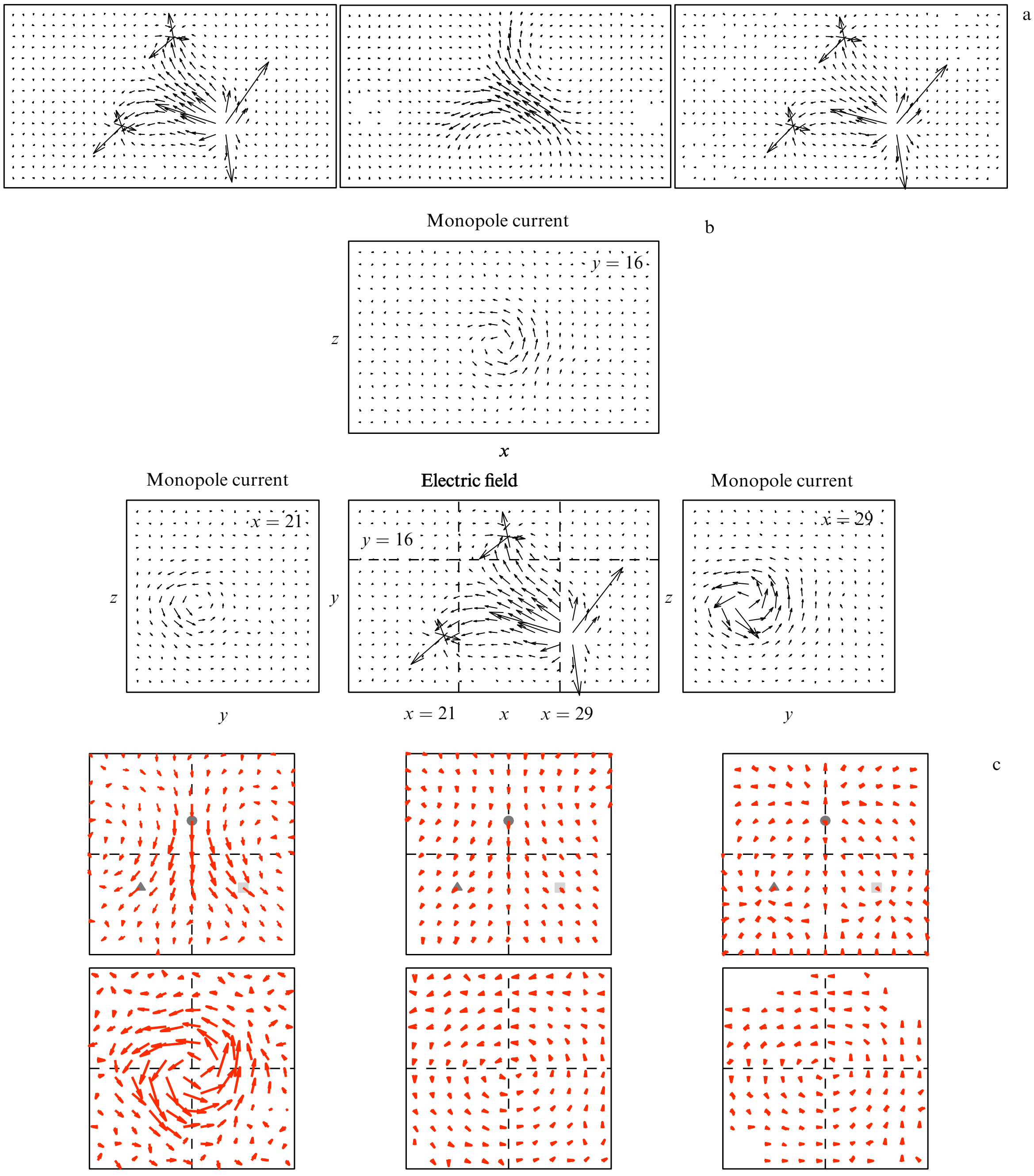

Figure 20. (a) From left to right: Abelian, monopole, and photon components of the electric field; (b) Abelian electric field and solenoidal magnetic current; (c) color electric field (upper row) and solenoidal magnetic current (lower row) at (from left to right) $T = 0.87\,T_c$, $T = T_c$, and $T = 1.25\,T_c$. The results were obtained within the full QCD.

The results discussed so far were obtained within the framework of full QCD. Our results for the Abelian action density in SU(3) gluodynamics are in qualitative agreement with the findings for the full QCD. Therefore, it is natural to assume the production mechanism of a string with a Y-shape to be the same both in QCD and in SU(3) gluodynamics.

5.3 Baryon structure at nonzero temperature

In this section we analyze the results obtained by us for magnetic currents and electric fields inside a baryon in the full QCD at nonzero temperature. Calculations were performed on a nonsymmetric $16^3 \times 8$ lattice. It is known that at a temperature above the critical temperature the string and solenoidal magnetic current in a quark–antiquark system vanish, and the Abelian electric field becomes a Coulomb field [4]. This effect was observed both in gluodynamics [65] and in full QCD [3, 66]. We have measured the Abelian baryon potential and have revealed that, as was to be expected, it increases linearly [5] as $T < T_c$, and rapidly smooths out for $T \geqslant T_c$.

[4] At present, numerical data do not permit us to distinguish Coulomb and Yukawa fields in a three-quark system unambiguously.
[5] The potential should first start to smooth out and tend toward a constant owing to the production of quarks from the vacuum at the distances exceeding the ones shown in the figure.

Figure 20c displays the monopole component of the electric field and the magnetic current in the plane orthogonal to the flux. It is seen that for $T < T_c$ the behaviors of both the electric field and the magnetic current closely resemble the behaviors of the respective quantities at zero temperature (Figs 20a, b). It should be noted that the operator P_{3q}^{Ab} applied at finite temperature, unlike the operator W_{3q}^{Ab}, has no Y-shaped connection. This stresses the fact that the Y-shape of the baryon structure is not related to the shape of the operator used for creating a three-quark state.

For a temperature $T > T_c$, the solenoidal magnetic current and the monopole component of the electric field have been discovered to vanish. As is seen from Fig. 19b, the Abelian action density has only three peaks in the absence of a string connecting the quarks. This picture complies with color deconfinement in the high-temperature phase.

6. Conclusions

The following results have been dealt with in this review:

• Abelian dominance has been confirmed for lattice QCD. In the MA projection, Abelian fields reproduce about 90% of the total string tension, which points to the leading role of Abelian degrees of freedom in the color confinement problem;

• the investigation of properties of the string responsible for confinement in the static quark – antiquark system has led to fulfilment of the dual Ampere law being revealed for the Abelian electric field and Abelian monopole currents. A value on the order of 0.3 fm has been obtained for the string width, and the width has been found not to depend upon the string length;

• the phase transition temperature has been calculated on a lattice with a record small spacing. In the chiral limit it amounts to $T_c \approx 170$ MeV in the theory with two light quarks, and to $T_c \approx 150$ MeV in QCD with *u*-, *d*-, and *s*-quarks;

• the effect of string breaking caused by the production of a quark – antiquark pair from the vacuum has been revealed at finite temperature ($T < T_c$). The parameters of the potential between the heavy quark and antiquark in the string breaking regime have been found. The contributions of monopoles to the string tension, the effective quark mass, and the distance at which the string breaks are in good agreement with the respective quantities obtained with the aid of non-Abelian correlators;

• studies of fields inside a baryon composed of three static quarks have revealed that in the color confinement mode there exists a Y-like field configuration corresponding to a three-particle potential which cannot be described as the sum of pair forces.

The authors are deeply grateful for numerous fruitful discussions to A I Veselov, H Ichie, Y Koma, Y Mori, Y Nakamura, D Pleiter, D A Sigaev, A A Slavnov, P V Uvarov, T Streuer, and H Stuben, together with whom most of the results presented were obtained. Discussions with G Bali, T Kovach, M Müller-Preussker, H Suganuma, and A Hart have been extremely helpful to the authors in implementing studies.

We are sincerely grateful to the staff members of the Joint Supercomputer Center (Moscow) and, especially, to A V Zabrodin for help in performing calculations on the Russian supercomputer MVS-1000M.

This work has been carried out with the partial support of: T.S. — JSPS grants 13135210 and (B) 15340073; M.I.P. and V.G.B. — RFBR grants 02-02-17308 and 01-02-17456, NNIO-RFBR grant 436 RUS 113/739/0, RFBR-NNIO grant 03-02-04016, as well as INTAS-00-00111 grant and the prize CRDF RPI-2364-MO-02, and M.N.Ch — fellowship JSPS P01023.

References

1. Bornyakov V et al. *Nucl. Phys. B: Proc. Suppl.* **106 – 107** 634 (2002); hep-lat/0310011
2. Bornyakov V et al. *Nucl. Phys. B: Proc. Suppl.* **119** 703 (2003); Mori Y et al. *Nucl. Phys. A* **721** 930 (2003)
3. Bornyakov V et al. *Nucl. Phys. B: Proc. Suppl.* **119** 712 (2003)
4. Ichie H et al. *Nucl. Phys. B: Proc. Suppl.* **119** 751 (2003); *Nucl. Phys. A* **721** 899 (2003)
5. Wilson K G *Phys. Rev. D* **10** 2445 (1974)
6. Jansen K, Sommer R *Nucl. Phys. B* **530** 185 (1998)
7. Peardon M *Nucl. Phys. B: Proc. Suppl.* **106 – 107** 3 (2002)
8. Ukawa A (CP – PACS and JLQCD Collab.) *Nucl. Phys. B: Proc. Suppl.* **106 – 107** 195 (2002)
9. Garden J et al. (UKQCD Collab.) *Nucl. Phys. B: Proc. Suppl.* **83 – 84** 165 (2000)
10. Aoki S et al. (CP – PACS Collab.) *Phys. Rev. Lett.* **84** 238 (2000)
11. Kanaya K et al. (CP – PACS Collab.) *Fortschr. Phys.* **50** 531 (2002)
12. Booth S et al. (QCDSF – UKQCD Collab.) *Phys. Lett. B* **519** 229 (2001)
13. Sommer R *Nucl. Phys. B* **411** 839 (1994)
14. 't Hooft G *Nucl. Phys. B* **190** 455 (1981)
15. Kronfeld A S et al. *Phys. Lett. B* **198** 516 (1987); Kronfeld A S, Schierholz G, Wiese U-J *Nucl. Phys. B* **293** 461 (1987); Brandstaeter F, Schierholz G,Wiese U-J *Phys. Lett. B* **272** 319 (1991)
16. Mandelstam S *Phys. Rep.* **23** 245 (1976); 't Hooft G, in *High Energy Physics: Proc. of the EPS Intern. Conf., Palermo, Italy, 23 – 28 June 1975* (Intern. Physics Series, issue 6, Ed. A Zichichi) (Bologna: Compositori, 1976)
17. Chernodub M N, Polikarpov M I, in *Confinement, Duality, and Nonperturbative Aspects of QCD* (NATO ASI Series, Ser. B, Vol. 368, Ed. van Baal P) (New York: Plenum Press, 1998) p. 387; hep-th/9710205 (1997); Haymaker R W *Phys. Rep.* **315** 153 (1999)
18. Bali G S et al. *Nucl. Phys. B: Proc. Suppl.* **42** 852 (1995)
19. Bali G S et al. *Phys. Rev. D* **54** 2863 (1996)
20. Polikarpov M I, Yee K *Phys. Lett. B* **316** 333 (1993)
21. DeGrand T A, Toussaint D *Phys. Rev. D* **22** 2478 (1980)
22. Kitahara S, Matsubara Y, Suzuki T *Prog. Theor. Phys.* **93** 1 (1995)
23. Hart A, Teper M *Phys. Rev. D* **58** 014504 (1998); **60** 114506 (1999)
24. Bornyakov V, Müller-Preussker M *Nucl. Phys. B: Proc. Suppl.* **106 – 107** 646 (2002)
25. Chernodub M N, Gubarev F V *Pis'ma Zh. Eksp. Teor. Fiz.* **62** 91 (1995) [*JETP Lett.* **62** 100 (1995)]
26. Hart A, Teper M *Phys. Lett. B* **371** 261 (1996)
27. Bornyakov V, Schierholz G *Phys. Lett. B* **384** 190 (1996)
28. Suzuki T, Yotsuyanagi I *Phys. Rev. D* **42** 4257 (1990)
29. Gribov V N *Nucl. Phys. B* **139** 1 (1978); Semenov-Tyanshanskiĭ M A, Franke V A, in *Zapiski Nauchnykh Seminarov Leningradskogo Otdeleniya Matematicheskogo Instituta im. V A Steklova AN SSSR* (Collection Notes of Scientific Seminars of the Leningrad Branch of the V A Steklov Mathematical Institute, AS USSR) Vol. 120 (Leningrad: Nauka, 1982) p. 159; Zwanziger D *Nucl. Phys. B* **378** 525 (1992); **399** 477 (1993)
30. Smit J, van der Sijs A J *Nucl. Phys. B* **355** 603 (1991)
31. Suzuki T et al. *Phys. Lett. B* **347** 375; Erratum **351** 603 (1995)
32. Haymaker R W et al. *Phys. Rev. D* **53** 389 (1996)
33. Bali G S, Schlichter Ch, Schilling K *Phys. Rev. D* **51** 5165 (1995); *Prog. Theor. Phys. Suppl.* (122) 67 (1996)
34. Koma Y et al. "A fresh look on the flux tube in Abelian-projected SU(*2*) gluodynamics", Preprint ITEP-LAT/2002-14; KANAZAWA-02-22; RCNP-Th02015; hep-lat/0210014
35. Gubarev F V et al. *Phys. Lett. B* **468** 134 (1999)
36. Glässner U et al. (SESAM Collab.) *Nucl. Phys. B: Proc. Suppl.* **53** 283 (1997); Allton C R et al. (UKQCD Collab.) *Phys. Rev. D* **60**

034507 (1999); Bolder B et al. (SESAM-TχL Collab.) *Phys. Rev. D* **63** 074504 (2001)
37. Güsken S *Nucl. Phys. B*: *Proc. Suppl.* **63** 16 (1998)
38. Aoki S et al. (CP-PACS Collab.) *Nucl. Phys. B*: *Proc. Suppl.* **73** 216 (1999)
39. Schilling K *Nucl. Phys. B*: *Proc. Suppl.* **83–84** 140 (2000)
40. Suzuki T, Chernodub M N *Phys. Lett. B* **563** 183 (2003); hep-lat/0207018; Preprint ITEP-LAT/2002-06
41. Lüscher M, Münster G, Weisz P *Nucl. Phys. B* **180** 1 (1981)
42. Bali G S, in *3rd Intern. Conf. on Quark Confinement and the Hadron Spectrum, Newport News, VA, 7–12 June 1998*, p. 17; hep-ph/9809351
43. Karsch F, Laermann E, Peikert A *Nucl. Phys. B* **605** 579 (2001)
44. Booth S et al. (QCDSF–UKQCD Collab.) *Phys. Lett. B* **519** 229 (2001)
45. Karsch F *AIP Conf. Proc.* **602** 323 (2001)
46. Edwards R G, Heller U M *Phys. Lett. B* **462** 132 (1999)
47. McLerran L D, Svetitsky B *Phys. Rev. D* **24** 450 (1981)
48. DeTar C et al. *Phys. Rev. D* **59** 031501 (1999)
49. Lüscher M, Weisz P *JHEP* **0207** 049 (2002)
50. Gao M *Phys. Rev. D* **40** 2708 (1989)
51. Bali G S et al. (SESAM-TχL Collab.) *Phys. Rev. D* **62** 054503 (2000)
52. Kaczmarek O et al. *Phys. Rev. D* **62** 034021 (2000)
53. Digal S, Petreczky P, Satz H *Phys. Lett. B* **514** 57 (2001)
54. Sommer R, Wosiek J *Phys. Lett. B* **149** 497 (1984)
55. Thacker H B, Eichten E, Sexton J C *Nucl. Phys. B*: *Proc. Suppl.* **4** 234 (1988)
56. Bali G S *Phys. Rep.* **343** 1 (2001)
57. Alexandrou C, de Forcrand Ph, Tsapalis A *Phys. Rev. D* **65** 054503 (2002)
58. Alexandrou C, de Forcrand Ph, Jahn O, hep-lat/0209062; *Nucl. Phys. B*: *Proc. Suppl.* **119** 667 (2003) (2003)
59. Takahashi T T et al. *Phys. Rev. D* **65** 114509 (2002); *Phys. Rev. Lett.* **86** 18 (2001)
60. Koma Y et al. *Phys. Rev. D* **64** 014015 (2001)
61. Komarov D A, Chernodub M N *Pis'ma Zh. Eksp. Teor. Fiz.* **68** 109 (1998) [*JETP Lett.* **68** 117 (1998)]
62. Kuzmenko D S, Simonov Yu A *Phys. Lett. B* **494** 81 (2000); hep-ph/0302071
63. Bornyakov V, Müller-Preussker M *Nucl. Phys. B*: *Proc. Suppl.* **106–107** 646 (2002)
64. Kamizawa S et al. *Nucl. Phys. B* **389** 563 (1993)
65. Peng Y, Haymaker R W *Phys. Rev. D* **52** 3030 (1995)
66. Feilmair W, Markum H *Nucl. Phys. B* **370** 299 (1992)